EUROPEAN ORGANIZATION FOR NUCLEAR RESEARCH
ORGANISATION EUROPÉENNE POUR LA RECHERCHE NUCLÉAIRE

EDMS Nr: 1031573
Group reference: EN-MME

CERN-EN-Note-2009- 001
26 August 2009

ANALYSIS AND DESIGN OF THE ACTUATION SYSTEM FOR THE LHC COLLIMATORS (PHASE I)

A. Bertarelli, A. Dallocchio, R. Perret, P. Smas

Abstract

In order to cope with the highly destructive particle beam of the LHC, the cleaning and collimation system must fulfill very severe requirements. The actuation system of the LHC Collimators is a key element to meet the specifications, particularly in terms of precision and reliability.
Each collimator jaw has to be moved with a very high accuracy to place the active surface at the required position with respect to the proton beam; at the same time the system must be adjustable and flexible to adapt to the uncertainties and variations in the beam tuning. In this note the general design of the actuation system for the various collimator designs is presented and particular emphasis is given to the analysis of the torque which the stepper motors must provide to move the jaws in and back and to the dynamical behaviour of the system in the event of malfunctioning when auto-retraction of the jaws is required. In the appendix, details are given on the estimated performances of the actuation system for different collimator types and orientations.

1 INTRODUCTION

The LHC cleaning and collimation system must cope with a highly destructive particle beam, implying a very demanding functional specification [1]; these requirements led to a quite complex mechanical system, to be implemented in two distinct phases. For the phase I only, which has been conceived for the early runs of the LHC operation when high robustness of the cleaning system is mandatory, more than 100 collimators with different designs, features and installation conditions are foreseen: among these objects the most challenging from the mechanical engineering point of view are the Secondary Collimators (TCSG).

Each collimator can be mounted with various azimuthal orientations to adapt to the beam optics. A general layout of a horizontal TCSG is given in Figure 1-1. More details on the general design can be found in [2].

The main goal of the actuation system of a LHC collimator is to ensure the precise movement of the jaw assemblies (a jaw assembly is made up by the jaw – the element designed to interact with the beam – and all its supporting components, including two axles, which connect the jaw metal support to the mobile tables). The required positioning accuracy must be a fraction of the typical beam size at the cleaning insertions. Each jaw assembly is driven by two stepper motors, via two precision roller screw sets, transforming the motor rotary movement into linear translation[1]. An auto-retraction system has been foreseen for most of the collimator types to allow the automatic retraction of the jaw assemblies to the full-out position in case both motors cannot provide the required torque (e.g. in case of power cut or low-level control failure): the efficiency of this feature depends on the detent torque of the stepping motors.

This technical note presents the design and the mechanical analysis of the LHC collimator actuating system. Reported calculations permit to determine the motor torque required to move each collimator jaw assembly over the full stroke range and to verify the ability of the system to drive back the jaws in case of motor failure. Only forces influencing the displacement of the collimator jaws are dealt with; other loads, namely those affecting the bearings and other components in directions other than that of movement, are not treated in this document.

Focus is mainly given to the TCSG[2] featuring a Carbon-fiber reinforced Carbon composite (C/C) jaw. Nevertheless other collimator types are also presented and analyzed, these include the types sharing the same actuation system with the TCSG, i.e. the Primary collimators (TCP) (only differing in the C/C jaw shape), the Tertiary Collimators type A (TCTA), having a Copper/Tungsten jaw, the Active Absorbers (TCLA and TCLP), with a Copper jaw and other designs with a special actuation system. The latter include the Transfer-line Collimators (TCDI), for which auto-retraction is proscribed and the units with a much different design induced by the requirement that both particle beams are encompassed by the collimator vacuum tank, namely the Active absorbers type A (TCLIA) and the Tertiary Collimators type B (TCTVB).

Detailed data and results for each collimator type and relevant orientations are given in the appendix.

---

[1] Precision roller screws are used for all the collimators types, with the exception of the TCDI having less stringent precision requirements and excluding auto-retraction. For these collimators a standard screw/nut assembly is used.

[2] The same TSCG design is also shared by the TCLIB (active absorbers for injection protection – type B).

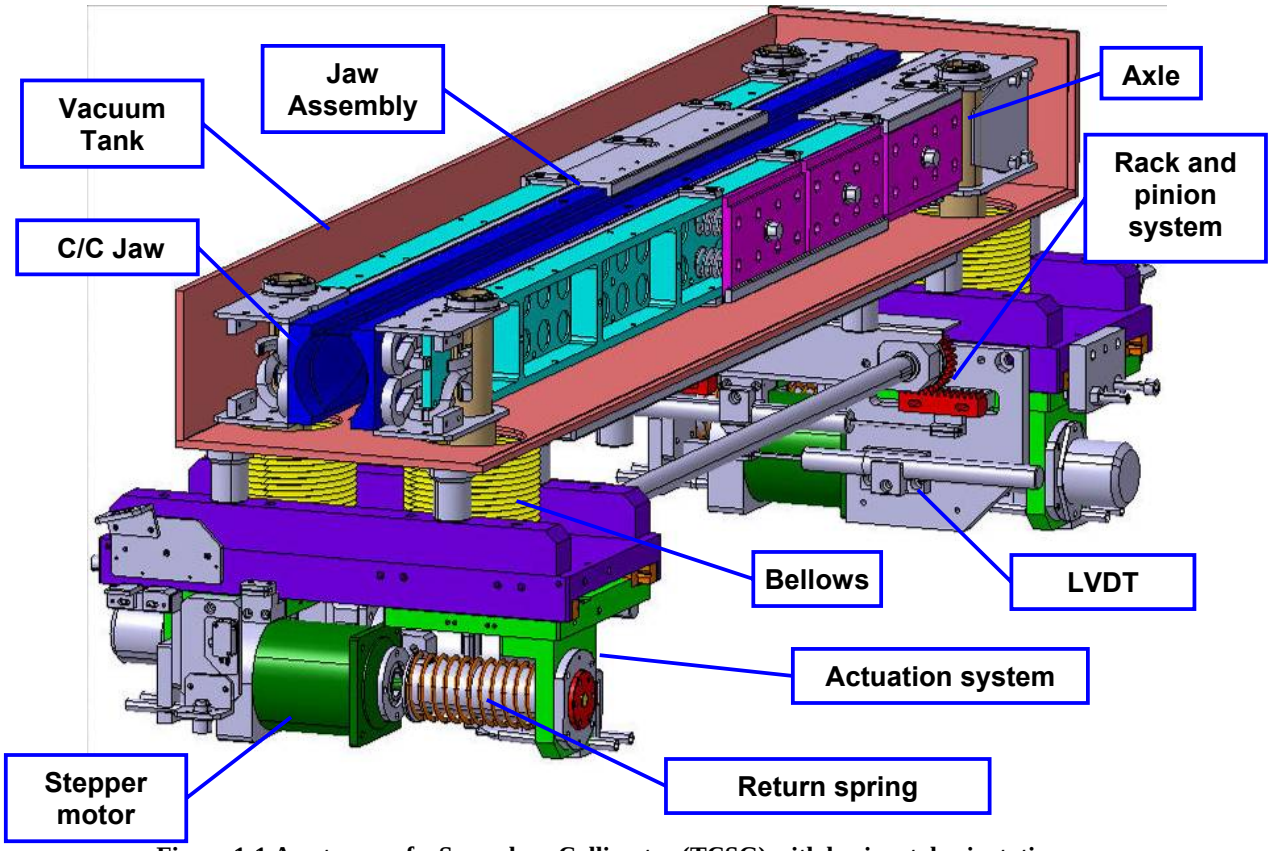

Figure 1-1 A cutaway of a Secondary Collimator (TCSG) with horizontal orientation

2 ACTUATION SYSTEM DESIGN

The most important requirements for the actuation system and the motorization, as given by the functional specification, are shown in Table 2-1.

Maximum full gap between jaws	60 mm
Minimum full gap between jaws	0.5 mm
Max jaw stroke past beam axis	5 mm
Knowledge of gap	50 μm
Jaw position control	10 μm
Jaw angle control	15 μrad
Reproducibility of setting	20 μm
Stepper-motor detent torque[3]	60-140 mNm
Minimum required lifetime	20000 cycles

Table 2-1 Main requirements and specifications for the actuation system

[3] The detent torque of a stepper motor designates the braking torque that the motor opposes to an external drive when it is not energized. This value was initially expected to be in line with LEP collimator stepper motors (~60 mNm). In fact, the detent torque of the chosen motor turned out to be much higher, up to ~140 mNm, due to the radiation-hardness requirements, higher delivered pull-in torque and the type of stepping motor chosen, i.e a hybrid motor. This motor has a permanently magnetized rotor which considerably increases the detent torque with respect to a variable reluctance motor.

Each jaw is independently supported on two axles and actuated by two stepper-motors (Figure 2-1). This allows both lateral displacement (with a nominal stroke of 30 mm plus 5 mm of extra-stroke to account for possible drifts in the beam orbit) and angular adjustment (the jaw assembly can pivot about each axle). Excessive tilt of the jaw is prevented by a rack and pinion system, which limits relative deviation in lateral displacement between the two axles to roughly 3 mm (i.e. 3 mrad).

In a TCSG, each motor directly drives, via a roller screw/nut set, a mobile table allowing the precise positioning of the jaw supporting axle. The linear screw is based on the principle of recirculating rollers, with internal axial play (as all plays are recovered by a preloaded spring – see below) [3]. Since the radiation hardness requirements prevent the use of a standard lubricant, to reduce the friction coefficient between nut and screw, the threaded shaft and the rollers are coated with a graphite layer applied by a special process called Lubodry® G [4]. To further reduce friction and increase screw endurance, a special radiation-hard grease is also used (Santovac 5GB [5]).

Each table is mounted on two low-friction linear bearings of the crossed-roller cage type. The hybrid stepping motor has a minimum of 200 steps per revolution; since the roller screw lead (pitch) is 2 mm, the linear advancement for each motor step is 10 μm. This value can be further reduced if the number of steps is increased (e.g. by a mini-step driver [6]). Vacuum tightness is guaranteed by four membrane bellows which can be bent sideways by up to 20 mm.

To ensure the expected lifetime of a collimator (~20 years) each table is required to perform at least 20000 full cycles (from full-out position to full-in position and backwards).

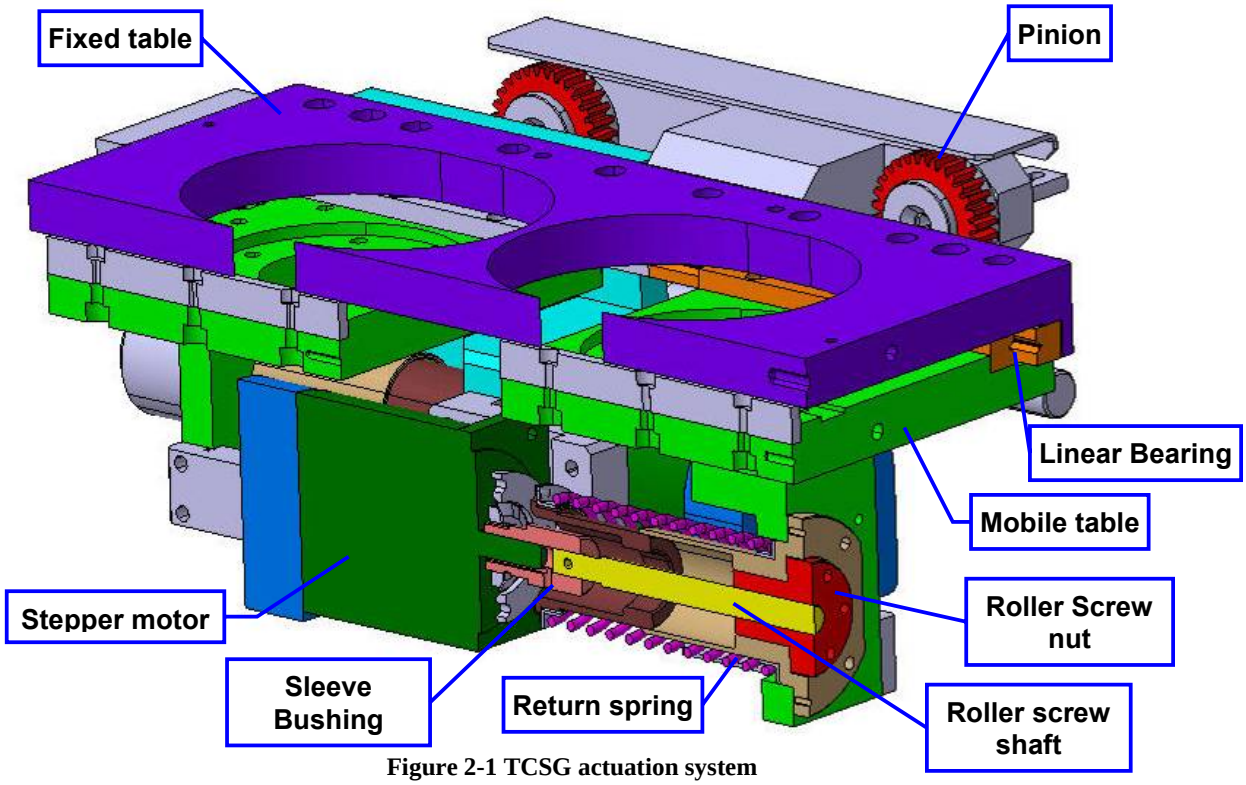

Figure 2-1 TCSG actuation system

The system is preloaded by compression springs to absorb all plays in the actuation system kinematical chain. The return spring was also chosen to obtain auto-retraction of the jaw in case the motor fails to provide the expected torque. The functionality of this feature depends on the motor detent torque (i.e. the “braking” torque it generates when externally driven). The position control is ensured by the motor encoder and by six linear position sensors (LVDT), overseeing mobile table

displacement and minimum gap between jaws. Mechanical stops and micro-switches are also foreseen to control jaw movement.

3 QUASI-STATIC ANALYSIS OF THE ACTUATION SYSTEM

One of the main goals of the analysis presented in this note is to estimate the torque to be provided by the stepper motor to drive in and back the collimator jaw assembly. As the expected linear velocities induced by the stepper motors are very low (typically 2 mm/sec), we can infer that linear and angular accelerations are negligible: it is then reasonable to ignore inertia forces and moments and adopt the quasi-static approach.

To facilitate the task, it is convenient to separate the forces acting on the jaw assembly and the mobile table from the moments acting about the axis of the screw and of the motor. Within the scope of this document, only forces acting along the movement direction are considered.

In the following analysis, x axis will denote linear displacement, its origin being at full-out position and positive displacements towards the full-in position. φ indicates angular displacement, angular values are positive when leading to positive displacements.

For sake of simplicity, we will assume external loads are either linear with displacement (e.g. elastic forces) or constant (weight and friction loads): in case of friction this might be a rather strong assumption, as we know that friction coefficients are different in static and dynamic conditions (e.g. stick-slip phenomena) and may vary with speed. However, this simplification is made necessary by the attempt to solve the problem analytically.

3.1 Forces acting on the moving parts

To derive the required motor torque, we must identify the loads acting along the direction of motion, either accelerating or decelerating the mobile table during its displacement. These forces are mainly the weight of the moving parts (more precisely, the component parallel to the displacement vector, depending on the collimator orientation), the return spring force, the bellows elastic force, the RF-transition elastic force and the friction forces.

Several relevant positions are specially regarded: these are the full-out position ($x = 0$ *mm*), the full-in position ($x = c_{max} = 35$ *mm*) and the nominal position ($c_{ref} = 28.5$ *mm*). The full-in position is placed 5 *mm* beyond the nominal beam axis. The nominal position is obtained assuming in working conditions a TCSG jaw is set at 7σ (σ is the RMS transverse beam size, i.e. *~0.2* mm in the cleaning insertions at 7 TeV).

Forces are positive when directed towards the full-in position.

3.1.1 Weight force

The total weight Q transferred to the roller screws and to the linear bearings is given by the contribution of the jaw assembly mass m_j and the mass of the axle and mobile table assemblies m_a:

$$Q = m_j g + m_a g \quad \textbf{(1)}$$

In order to cope with the beam optics, each collimator must be mounted with a specific azimuthal orientation of the jaw. Mechanically, this requirement is met by rotating the full collimator tank; four different collimator supports exist (0º, 45º, 90º and 135º), each one allowing an adjustment range of several degrees. Within the scope of this analysis, the orientation angle range can be taken as:

$$-90^\circ \le \beta \le 90^\circ \quad \textbf{(2)}$$

The orientations we will specially regard are 0º, 45º, -45º, 90º, -90º. According to the azimuth, a part of the weight will be transferred to the roller screws and the reminder taken by the fixed tables via the linear bearings. The weight component acting on the axis of each roller screw (two per jaw assembly) is given by:

$$W = \frac{Q}{2}\sin\beta \qquad \textbf{(3)}$$

As we have two tables per jaw assembly, only half of Q is taken. Positive β means the weight is driving the jaw to the full-in position and vice versa.

3.1.2 Return spring force

The compression spring between the motor and the table assembly is used to recover all the plays within the mechanical chain from the roller screw to the mobile table and to allow the auto-retraction of the collimator jaw in a case of emergency.

L_{ro} is the spring length at the full-out position ($x=0$). The minimum spring length L_{rc} corresponds to the full-in position (i.e. $x=c_{max}$):

$$L_{rc} = L_{ro} - c_{\max} \qquad \textbf{(4)}$$

The spring force F_r is a linear function of the stroke and can be written as:

$$F_r(x) = -K_r\left(L_0 - L_{ro} + x\right) = F_{r0} - K_r x \qquad \textbf{(5)}$$

where L_{ro} denotes the mounted spring length, K_r is the spring ratio and L_0 the free length. F_{r0} is the spring force (negative) at the full-out position.

3.1.3 Bellows force

Stainless steel (AISI 316 LN) membrane bellows are mounted between the tank bottom cover and the mobile table, encompassing the axle (Figure 1-1), to ensure the vacuum tightness of the collimator. Contributions to the forces on the mobile table are due to its lateral stiffness and to the lateral load induced by vacuum when the bellows is bent sideways. Nominal bellows position corresponds to the straight configuration without bending.

Bellows permitted lateral stroke c_{bl} is 20 mm: at this position the lateral force induced by vacuum F_{pl}, is usually provided by bellows suppliers [7] [8]. We assume the effect of vacuum to vary linearly with lateral stroke: in this case an equivalent lateral vacuum spring rate can be calculated:

$$K_{bp} = \frac{F_{pl}}{c_{bl}} \qquad \textbf{(6)}$$

Total lateral bellows spring rate is given by:

$$K_{bl} = K_{bn} + K_{bp} \qquad \textbf{(7)}$$

where K_{bn} is the nominal lateral spring rate provided by suppliers' data sheets.

As above, bellows lateral force F_b is a function of stroke x:

$$F_b(x) = -K_{bl}\left(x - L_{bn}\right) = F_{b0} - K_{bl}x \qquad \textbf{(8)}$$

where $L_{bn}=19\ mm$ denotes the nominal bellows position with respect to full-out position.

3.1.4 Friction force due to linear bearings

Each mobile table is supported on two linear bearings. For the TCSG-type collimators the chosen bearings are of the crossed-roller cage type; all bearing components (rails, cages and rollers) are corrosion resistant. No lubrication is foreseen because of the highly radioactive environment[4].

Each mobile table is kept in place by set-screws which preload the linear bearings (Figure 3-1), so allowing any type of mounting (horizontal, vertical, skew) and loading.

The maximum admissible preload per screw F_{vs} is given by the following formula:

$$F_{vs} = p_{r\max} n_r C \quad \textbf{(9)}$$

Where C denotes the permissible load per roller, n_r is the number of active rollers per setscrew, (obtained by dividing the distance between two preload screws L_1 by the roller pitch t):

$$n_r = \frac{L_1}{t} \quad \textbf{(10)}$$

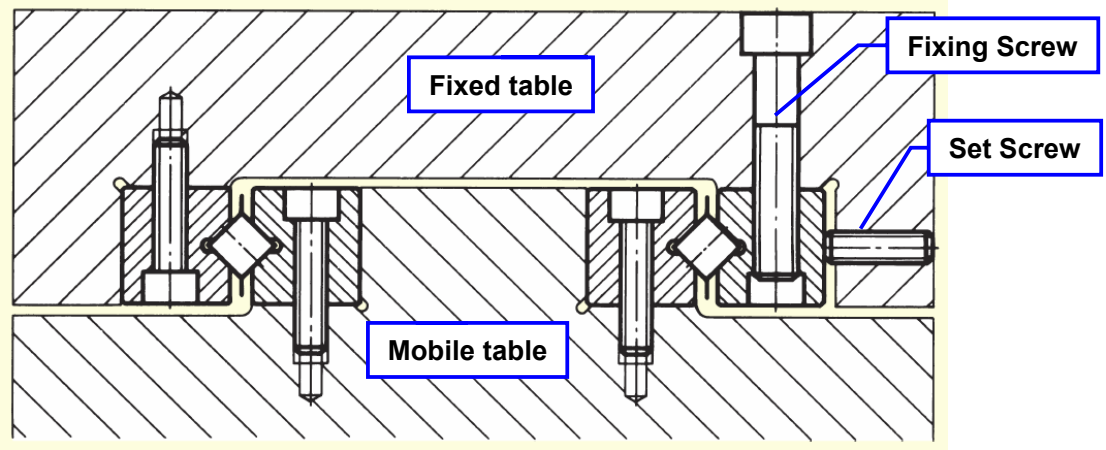

Figure 3-1 Linear bearing assembly mounting scheme (Source Schneeberger)

And p_{rmax} is 20% (its usual range is 2 to 20%).

The maximum admissible preload force per rail is then:

$$F_{rt\ Max} = n_{vs} F_{vs} \quad \textbf{(11)}$$

Where n_{vs} is the number of set-screws per rail.

Typically, maximum screw tightening torque can be calculated via a tightening coefficient a_{vs} which depends on the screw thread [10] [11]:

$$M_{vs} = F_{vs} a_{vs} \quad \textbf{(12)}$$

---

[4] In order to minimize wear risks on the roller and rail bearing surfaces, a graphite-based dry lubricant was tested. In spite of its good lubricating properties, drastically reducing surface wear, this product could not be applied because the radioactive and humid environment enhances graphite induced corrosion on unprotected aluminum roller cage surfaces and brass components (only present in TCTVB/TCLIA linear bearings featuring an anti-creeping system) [9].

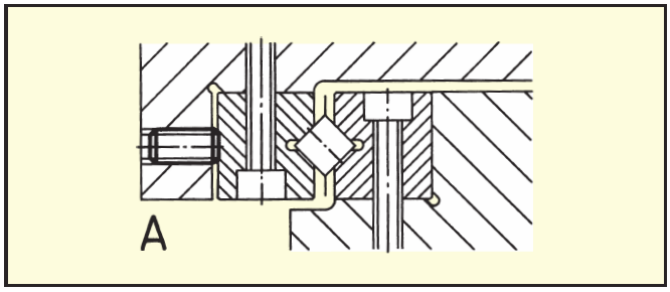

Figure 3-2 Mounting scheme of a crossed-roller cage linear bearing (source Schneeberger)

In our case, to better control the applied preload and avoid the typical dispersions due to tightening torque, friction coefficients etc., the linear bearing assembly is put into place by a specially designed mounting tool, which applies the required preload in a controlled way thanks to compression springs, before tightening the fixing screws.

In this case the actual preload force per rail is:

$$F_{rt} = n_{lb} K_{lb} L_{lb} \tag{13}$$

Where n_{lb} is the number of preloading springs of the tool (*2*), K_{lb} is the spring ratio (*80 N/mm*) and L_{lb} the spring allowed compression (*8.5 mm*).

The jaw assembly is supported by means of two mobile tables. Each table slides on two linear bearings. Hence, each linear bearing rail transmits a quarter of the component of the mobile assembly weight normal to the sliding plane, plus the preload force. Conservatively assuming the highest friction coefficient foreseen for these bearings (η_t = 0.003) and the whole weight regardless of the orientation angle, friction force per table is given by:

$$F_{ft} = \left| 2\eta_t \left(F_{rt} + \frac{Q}{4} \right) \right| \tag{14}$$

3.1.5 Friction force due to longitudinal RF contacts

The longitudinal RF contact system[5] is based on a series of Ag-coated Copper-Beryllium contact strips. A cross-section of the assembly is shown in Figure 3-3. Values of the geometrical dimensions indicated in Figure 3-3 are given in Table 3-1. The contact strips are mounted on the clamps of each jaw assembly. When jaws are moved, contact strip fingers slide on the longitudinal top and bottom stainless-steel rails. Each longitudinal rail is elastically supported on 8 springs of stiffness K_s=*1.591 N/mm*. The free length Ls_0 of these springs is 26 mm.

Reference surface height h_{nom} [mm]	Half height of the jaw h_{jaw} [mm]	Thickness of the longitudinal rail t_r [mm]	Base position of the rail hb_{rail} [mm]	Pin position h_{pin} [mm]
60	44	1.5	7	5.5

Table 3-1 Dimension values for the longitudinal RF contact system

[5] All collimator types are equipped with an RF contact system excepted the TCDI.

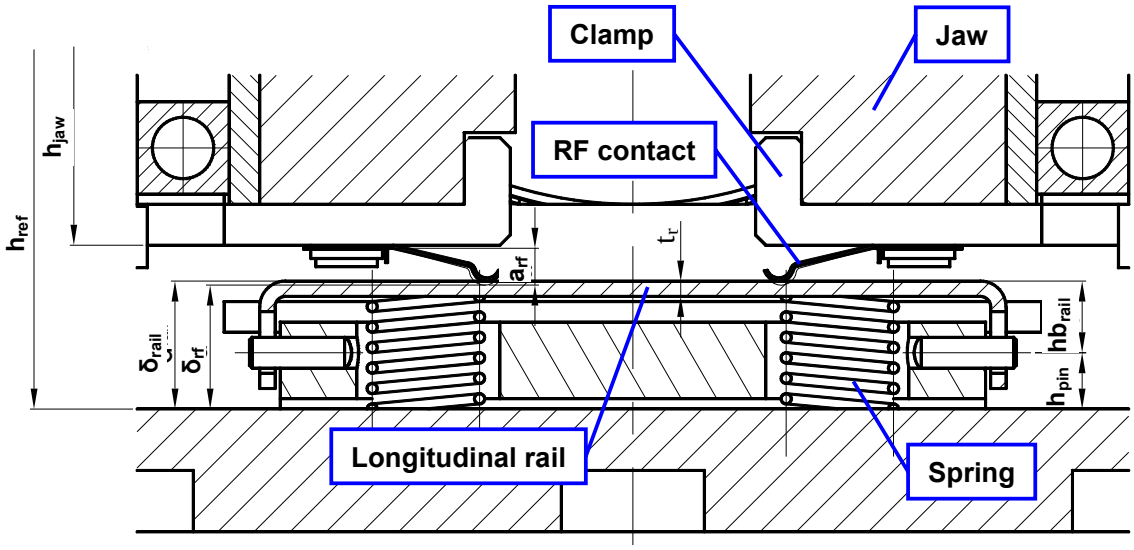

Figure 3-3 Longitudinal RF contact scheme

The total spring rate per rail is then:

$$F_{Ts} = 8K_s = 12.7\frac{N}{mm} \tag{15}$$

Every jaw assembly has 4 clamps, each one equipped with two contact strips of different length (type 1 and type 2) (Figure 3-4). Each strip encompasses several contact fingers as shown in Figure 3-5. Geometrical data for the contact strips are given in Table 3-2; Young's modulus of the contact strips Copper-Beryllium alloy is E_{CuBe}=135GPa [12].

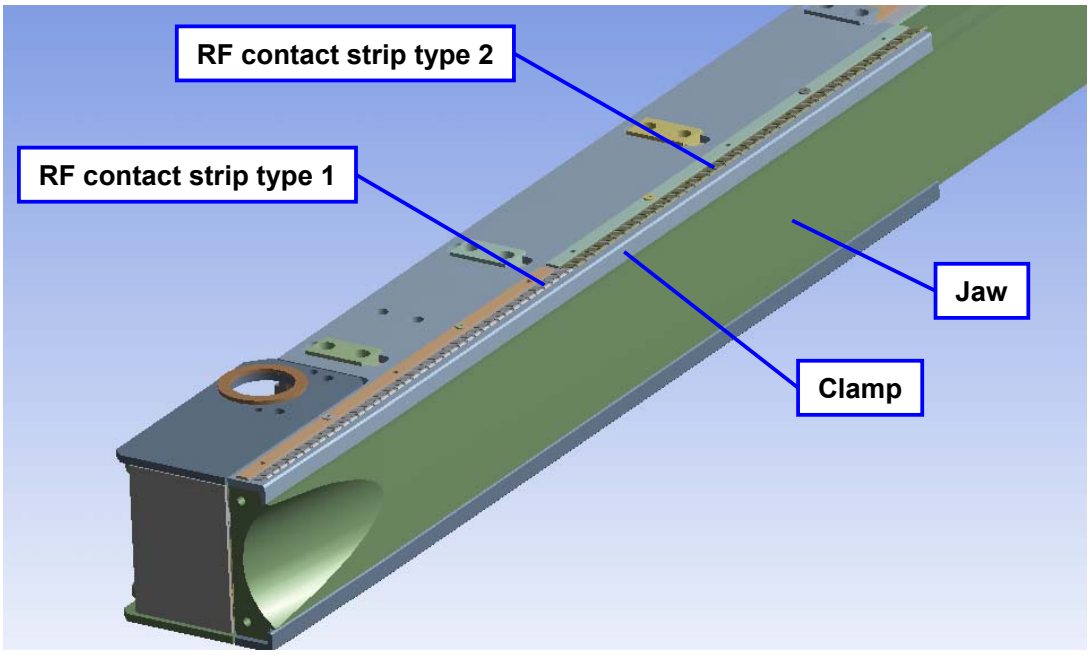

Figure 3-4 Mounting scheme of RF contact strips on a TCSG jaw (1 clamp shown)

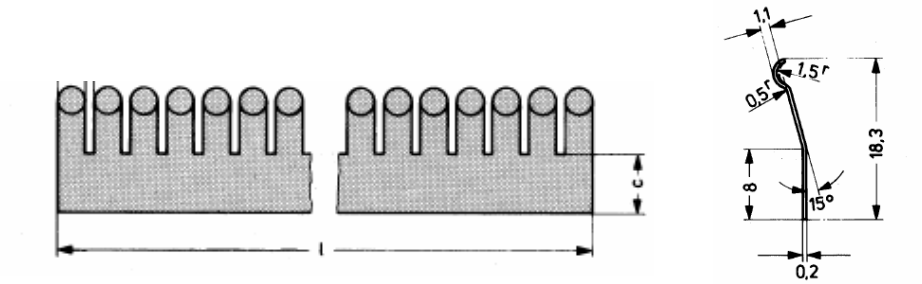

Figure 3-5 RF Contact strip

RF finger width b_{rf} [mm]	RF strip thickness t_{rf} [mm]	Gap between fingers g_{rf} [mm]	Free height of the RF strip a_{rf} [mm]	RF finger length w_{0rf} [mm]	Type 1 strip length $L1_{rf}$ [mm]	Type 2 strip length $L2_{rf}$ [mm]
3	0.15	1	3.85	10.3	276	316

Table 3-2 RF contact strips data

Since each longitudinal rail is in contact with four strips of both types, the number of RF fingers per rail can be calculated as:

$$n_{rf} = 4\frac{L1_{rf} + L2_{rf}}{b_{rf} + g_{rf}} \quad \textbf{(16)}$$

The linear stiffness of the RF finger can be approximated as the ratio of the bending force to the deflection of the RF finger (treated as an elastic beam clamped at one end):

$$K_{rf} = \frac{3E_{CuBe}I_{rf}}{w_{rf}^{3}} = 0.5\frac{N}{mm} \quad \textbf{(17)}$$

where I_{rf} is the moment of inertia of the RF finger ($b_{rf}\,t_{rf}^{3}/12$) and the equivalent RF finger length w_{rf} takes into account the correction coefficient cor=*-1.5mm* to compensate for the elbow softening:

$$w_{rf} = w_{0rf} + cor \quad \textbf{(18)}$$

Total RF contact stiffness becomes:

$$K_{Trf} = n_{rf}K_{rf} = 297\frac{N}{mm} \quad \textbf{(19)}$$

Since the relative positioning of the jaw assembly with respect to the tank cover plates might be affected by relatively large errors[6], it is interesting to study the behavior of the longitudinal RF contact system with respect to this positioning error; therefore, we assume that the reference distance h_{ref}, i.e. the distance of the internal face of the tank cover plates from the jaw plane of symmetry, is a function of the error parameter *err*:

[6] These errors are mainly due to the flatness tolerance of the tank cover plates and to the tolerance chain defining the position of the jaw assembly with respect to the collimator tank.

$$h_{ref}(err) = h_{nom} - err \tag{20}$$

The RF finger free position (with respect to the internal face of the cover plate) δ_{rf} (see Figure 3-3) is hence also a function of *err*:

$$\delta_{rf}(err) = h_{ref}(err) - h_{jaw} - a_{rf} \tag{21}$$

The rail position under the sole effect of spring preload is given by (see Figure 3-3):

$$\delta_{rail} = h_{pin} + hb_{rail} \tag{22}$$

Hence, the in-place length of the springs become:

$$Ls_p = \delta_{rail} - t_r \tag{23}$$

The total spring initial preload is given by:

$$Fp_s = K_{Ts}\left(Ls_0 - Ls_p\right) = 191N \tag{24}$$

Contact between RF fingers and the longitudinal rail exists if the theoretical interference value:

$$i(err) = \delta_{rail} - \delta_{rf}(err) \tag{25}$$

is positive. Otherwise, there is no contact and the friction force is zero.

In case of contact, the rail springs are not additionally compressed as long as:

$$K_{Trf}\, i(err) \le Fp_s \tag{26}$$

In this case only the RF fingers are bent and the rail does not move.

If equation (26) is not satisfied, then both rail springs and RF fingers are compressed (see Figure 3-6). In this case the force equilibrium equation leads to the following relation for the rail displacement (additional spring compression):

$$x_r(err) = \frac{K_{Trf}\, i(err) - Fp_s}{K_{Trf} + K_{Ts}} \tag{27}$$

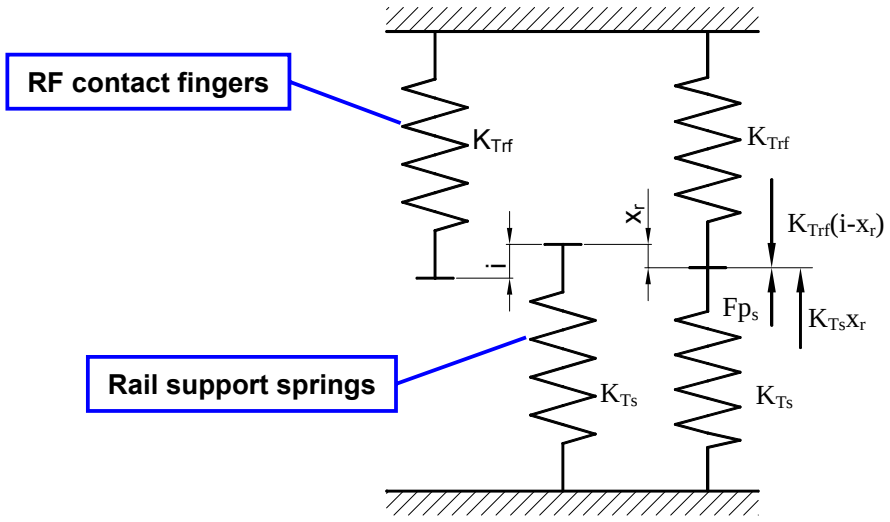

Figure 3-6 Scheme of the RF contact and rail springs interaction (presented, on the left side, the free position of each component and, on the right side, the situation in case eqn. 26 is not satisfied)

From Figure 3-6, we also see that the RF finger deflection is given by:

$$y_{rf}(err) = i(err) - x_r(err) \tag{28}$$

The actual contact force can now be calculated as:

$$F_{rf}(err) = Fp_s + K_{Ts}x_r(err) = K_{Trf}y_{rf}(err) \tag{29}$$

In nominal conditions, i.e. $err = 0$, the finger compression is $y_{rf}(0) = 0.35\ mm$ and the contact force is:

$$F_{rf}(0) = 104\,N \tag{30}$$

The rail maximum travel before it touches the cover plates is $c_r = 2.5\ mm$, then:

$$x_r(err) \le c_r \tag{31}$$

If the positioning error is larger than this value, all the additional compression will be taken by the RF fingers. Plots of the RF compression travel and of the RF contact force as a function of error are given in Figure 3-7 and Figure 3-8, respectively.

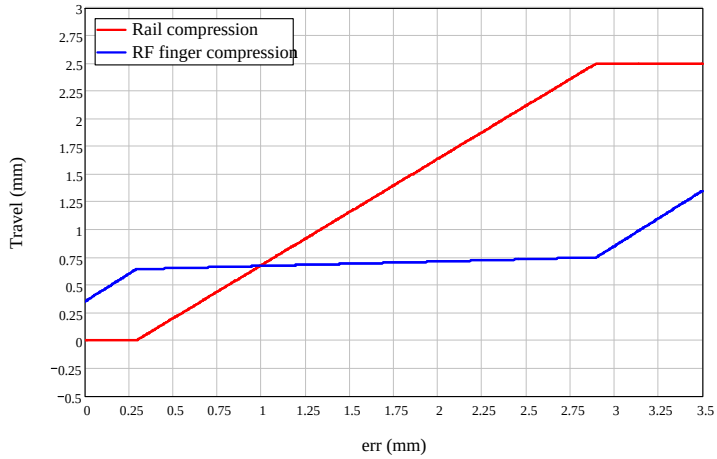

Figure 3-7 Compression of the RF system elastic components as a function of positioning error

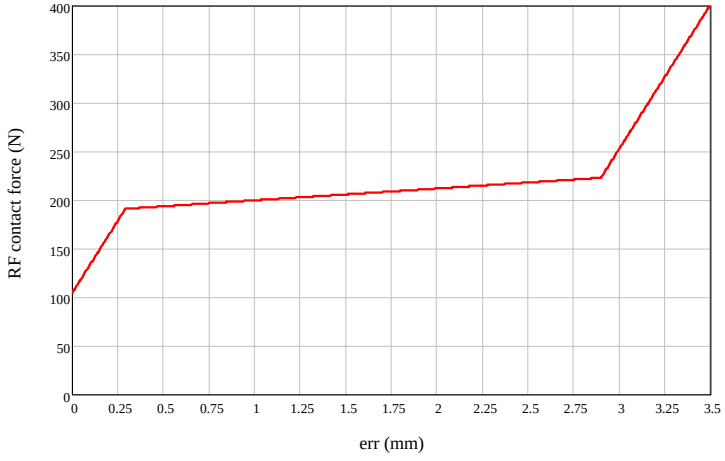

Figure 3-8 RF system contact force (per rail) as a function of positioning error

The friction force per each of the 4 tables, taking into account top and bottom contacts, is:

$$F_{fr}(err) = \left| 2\mu_{rf} \frac{F_{rf}(err)}{4} \right| \quad \textbf{(32)}$$

Where μ_{rf} denotes the friction coefficient between the stainless steel rail and the Ag-coated CuBe fingers: as contact is in vacuum, we conservatively assume $\mu_{rf}=0.6$.

Since the contribution to the positioning error due to tolerances in the localization of the jaw assembly with respect to the collimator tank is opposed in sign on top and bottom rails, this term gives no contribution to the friction force (provided the force remains in one of the first two legs of Figure 3-8), then the main remaining error source is the tank cover flatness tolerance. From production experience, we know that this error tends to be smaller or equal to 1 mm, therefore the maximum friction force per table is given by:

$$F_{frMax} = F_{fr}(1mm) = 60N \quad \textbf{(33)}$$

3.1.6 RF transition elastic force

To ensure the Radio-Frequency continuity between the Carbon-Carbon jaw and the vacuum flanges of the collimator tank and beam pipe, flexible RF transitions have been designed and mounted on each of the jaw ends. These transitions are essentially made by a system of long RF contact fingers ("comb") ensuring a continuous electrical path between the flat surfaces of the jaw and the circular flanges. During jaw movements these fingers are bent sideways generating a certain elastic force, which is zero when the fingers are aligned with the flange. On top of elastic deformation, during movement, each finger undergoes a certain degree of sliding between the internal and external ring of the flanges: this will obviously generate friction forces which we neglect in this analysis.

Each comb has 15 long RF fingers made of CuBe alloy (UNS C 17410 TH02); the Young's modulus is *139* GPa. The undeformed fingers position is L_{t0}=8.8 mm. From finite element simulations [13], we have found that the elastic force at full-in position is roughly F_{tMax} = 18 N. Assuming a fully linear

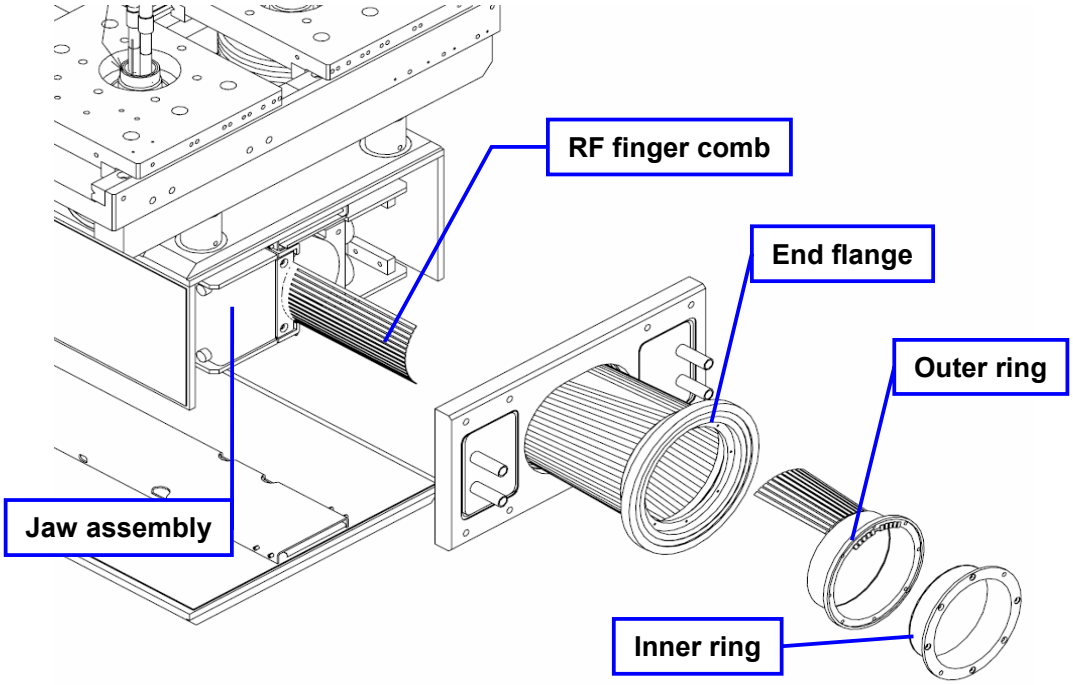

3-9: Exploded view of a TCSG RF transition

behaviour, we can calculate the RF transition elastic stiffness:

$$K_t = \frac{F_{tMax}}{c_{\max} - L_{t0}} = 0.69 \frac{N}{mm} \tag{34}$$

The force as a function of the jaw position is then given by:

$$F_t(x) = -K_t\left(x - L_{tf\,0}\right) = F_{t0} - K_t x \tag{35}$$

3.1.7 Total quasi-static forces

To calculate the total force required to drive in and back the jaw assembly, we must counteract all forces acting on the jaw assembly. The quasi-static force $F_{qs}(x)$ to be provided in order to move in (positive direction) the jaw assembly is a function of the stroke and is equal and opposed to the sum of all service load components:

$$F_{qs}(x) = \left|F_{fr}\right| + \left|F_{ft}\right| - F_b(x) - F_r(x) - F_t(x) - W(\beta) \tag{36}$$

The RF contact friction force F_{fr} and the linear bearing friction force F_{ft} in (36) are always positive since they are opposed to the motion direction. The weight force component W transmitted to the roller screw is a function of the orientation angle β.

It is useful to separate, in (36), the linear part from the constant term. We obtain then:

$$F_{qs}(x) = F_0 + K_T x \tag{37}$$

Where $F_0 = F_{fr} + F_{ft} - F_{b0} - F_{r0} - F_{t0} - W(\beta)$ is the quasi-static force required to start moving in the jaw at full-out position and $K_T = K_r + K_{bl} + K_t$ is the total stiffness.

The force required to move back the jaw can be calculated likewise. The only difference with respect to previous equation is given by the reversal of the direction of friction forces.

$$F'_{qs}(x) = -\left|F_{fr}\right| - \left|F_{ft}\right| - F_b(x) - F_r(x) - F_t(x) - W(\beta) = F'_0 + K_T x \tag{38}$$

In this case, a positive value means the motor must "brake" the table, which tends to move outwards.

In Figure 3-10, the resultant forces required to drive the jaw in and out are plotted versus stroke along with the return spring and bellows forces for a TCSG having stiff springs and a vertical orientation (weight opposing the jaw opening).

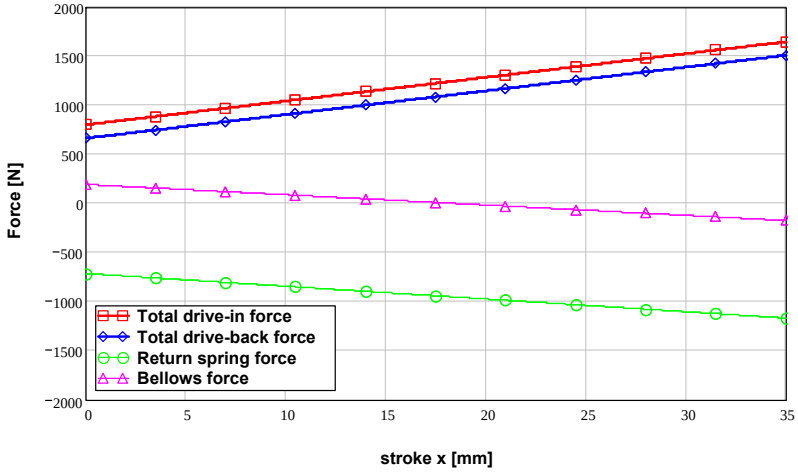

Figure 3-10 Drive-in and drive-back forces for a TCSG collimator, with β= -90° and stiff springs

3.2 Quasi static torque

As it can be seen from Figure 3-11, the actuation system of a LHC collimator is composed both of translating and of rotating parts: in order to analyze it correctly, we must reduce the problem to one with a single degree of freedom, i.e. the rotation angle φ or the linear displacement x.

To do so, we need to recall the basic kinematic relation of a screw, transforming rotation into translation and vice-versa, i.e.:

$$d\varphi = \frac{2\pi}{p} dx \tag{39}$$

Where p is the lead (or pitch) of the screw.

To calculate the quasi-static torque to be applied to the screw shaft and to obtain the force necessary to drive in or out the jaw assembly, we must remember that part of the work done by the motor to move the system is dissipated by friction between the screw and the nut. This is usually taken into account by introducing the concept of efficiency, defined as the ratio between the work required to move the load in the absence and in the presence of friction.

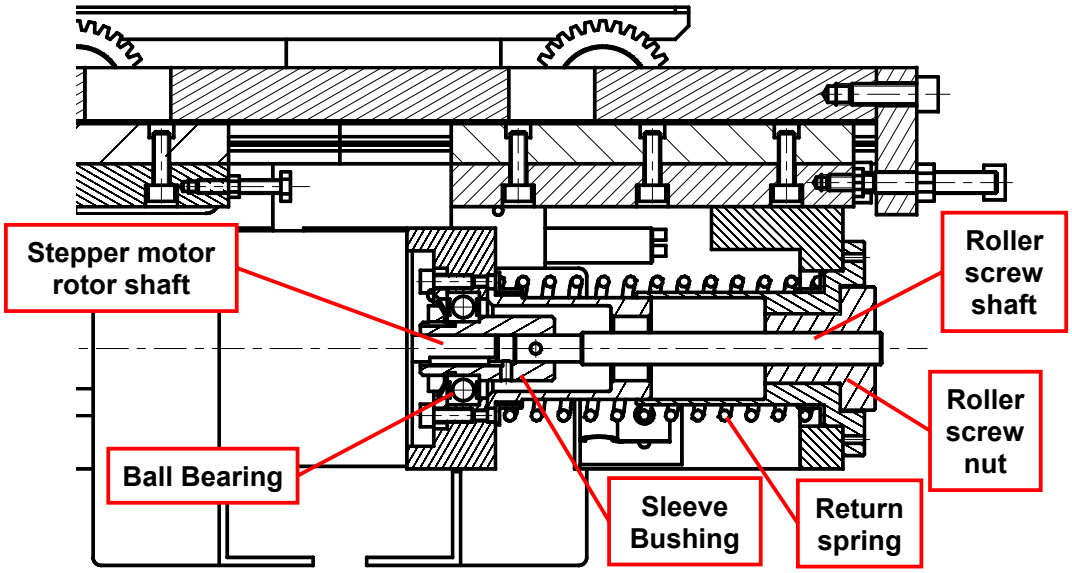

Figure 3-11 Cross-section of the TCSG actuating system

When the direction of the motion is opposed to the force exerted by the service loads on the nut (i.e. the work of the thrust generated by the screw on the nut is positive), we talk of **direct efficiency** (η). Introducing M_{fS} as the torque (positive) dissipated by friction between screw and nut and bearing in mind equation (39), we can write:

$$\eta = \frac{\frac{Fp}{2\pi}}{\frac{Fp}{2\pi} + M_{fS}} \tag{40}$$

The usual formula for the ***direct efficiency*** of a roller screw is given by [3]:

$$\eta = \frac{1}{1 + \frac{\pi \mu_s d_0}{p}} \tag{41}$$

where d_0 denotes the nominal diameter of the screw and μ_s represents the friction coefficient between rollers, nut and screw.

For normal applications, it is customary to apply a certain reduction coefficient, so that ***practical direct efficiency*** η_p becomes [3]:

$$\eta_p = 0.9\eta \tag{42}$$

When the resultant of the service loads on the nut has the same direction as the displacement, the force exerted by the screw must counteract this resultant, i.e. its work is negative. In this case we talk of ***indirect efficiency*** (η'); for a positive load F, it is defined as:

$$\eta' = \frac{\frac{Fp}{2\pi} - M_{fS}}{\frac{Fp}{2\pi}} \tag{43}$$

The formula for indirect efficiency of a power screw is then given by:

$$\eta' = 2 - \frac{1}{\eta} \tag{44}$$

It is immediate to see that when the direct efficiency is less than 0.5, the indirect efficiency becomes negative. This means that the friction torque dissipated by the screw to turn would be higher than the torque produced by the service load, hence this load cannot generate by itself any rotation about the screw axis, in other words the screw is self-locking. In our application, this means no auto-retraction is possible.

It is also important to note that the concept of direct and indirect efficiency is, in principle, independent of motion direction; in fact the service load on the nut might be in the direction of motion both when moving back and when moving in. In our application the quasi-static force is usually positive, i.e. we must use direct efficiency when moving in and indirect efficiency when moving back; however, should $F_{qs}(x)$ become negative, we would have to supply a negative (braking) force when moving in the jaw: in this case indirect efficiency must be used to calculate the drive-in torque and direct efficiency for the drive-back torque.

3.2.1 Ball Bearing friction moment

The friction moment induced by the ball bearing supporting the screw (see Figure 3-11) can be calculated in several ways according to the degree of accuracy which is sought [13]. In our case, we choose the simplest method, which has the advantage of expressing the friction moment as a linear function of the axial force, hence simplifying the dynamic analysis. The quasi-static friction torque when moving in is:

$$M_{bqs}(x) = \left| \mu F_{qs}(x) \frac{d}{2} \right| = \left| \mu \frac{d}{2} \left(F_0 - K_T x \right) \right| \tag{45}$$

and the quasi-static bearing friction moment when moving back:

$$M'_{bqs}(x) = \left|\mu F'_{qs}(x)\frac{d}{2}\right| = \left|\mu\left(F'_0 - K_T x\right)\frac{d}{2}\right| \quad \textbf{(46)}$$

The friction coefficient μ depends on the type of bearing, which is a four-contacts ball bearing for the TCLIA and TCTVB and a standard deep-groove ball bearing in all other cases. Numerical values are given in the appendix.

3.2.2 Drive-in and drive-back torque

The torque to be supplied by the motor to drive in or back the system in quasi-static conditions is given by the sum of the term necessary to counteract the service load on the screw nut ($F_{qs}(x)$ or $F'_{qs}(x)$), the friction torque dissipated between screw and nut $M_{fS}(x)$ and the friction torque dissipated by the ball bearing $M_{bqs}(x)$. The following formula is valid for positive displacements both for direct and indirect motion and (in case of back-driving F_{qs} and T_{qs} must be replaced by F'_{qs} and T'_{qs} respectively). Positive signs are taken before the friction terms when the service load has the same sign of the motion direction.

$$T_{qs}(x) = \frac{F_{qs}(x)p}{2\pi} \pm \left|M_{fS}(x)\right| \pm \left|M_{bqs}(x)\right| \quad \textbf{(47)}$$

As above, it is convenient to separate the constant from the linear term. Making use of the definitions of efficiency, the torque required to move in the jaw becomes:

$$T_{qs}(x) = T_0 + K_{\varphi e}x \quad \textbf{(48)}$$

T_0 is the quasi-static drive-in torque at full-out position and is given by:

$$T_0 = \begin{cases} \dfrac{F_0 p}{2\pi\eta_p} + \dfrac{\mu d}{2}F_0 & \text{if } F_{qs}(\mathrm{x}) \geq 0 \\ \dfrac{F_0 p\eta'}{2\pi} - \dfrac{\mu d}{2}F_0 & \text{otherwise} \end{cases} \quad \textbf{(49)}$$

$K_{\varphi e}$ is the drive-in torque per unit of displacement, proportional to an equivalent torsional stiffness.

$$K_{\varphi e} = \begin{cases} \dfrac{K_T p}{2\pi\eta_p} + \mu\dfrac{d}{2}K_T & \text{if } F_{qs}(\mathrm{x}) \geq 0 \\ \dfrac{K_T p\eta'}{2\pi} - \mu\dfrac{d}{2}K_T & \text{otherwise} \end{cases} \quad \textbf{(50)}$$

Equation (50) implies that if there is a change in the direction of the service load during the closing phase, the slope of the torque curve will change.

As said above, given that the accelerations which are expected in the direct motion are very small (typical jaw velocities are in the range of 1 mm/s), we may consider that the quasi-static torque required to drive in the system can be confounded with total dynamic torque.

Likewise, the quasi-static torque required to move back the jaw is given by:

$$T'_{qs}(x) = T'_0 + K'_{\varphi e}x \quad \textbf{(51)}$$

T'_0 and $K'_{\varphi e}$ are defined in a similar manner. As in equation (38), a positive value of T'_{qs} means the motor is braking the system.

4 DYNAMIC ANALYSIS OF AUTO-RETRACTION

The system behavior in case of auto-retraction is not as straight-forward as in direct motion, where the motor directly imposes displacement and accelerations are very small; back-driving dynamic performances essentially depend on the equilibrium between inertia forces, elastic forces, friction forces and weight component. A detailed analysis to predict auto-retraction performances is presented in this chapter.

4.1 Equivalent dynamic model for the actuation system

We know, by definition of inverse efficiency, that the following work identity applies:

$$T'd\varphi = \eta' F' dx \qquad \textit{(52)}$$

Equation (52) states that, in case of auto-retraction, the amount of work done by any back-driving load *F'* acting on the table (i.e. inertia, elastic or friction forces) which can be converted into rotary work is proportional to the indirect efficiency, the remainder of the work done by *F'* being dissipated into heat.

Introducing equation (39) into (52) we obtain:

$$T' = \eta' F' \frac{p}{2\pi} \qquad \textbf{(53)}$$

Equation (53) expresses how any back-driving force *F'* is converted into an equivalent torque *T'*.

4.2 Equation of motion

In virtue of equation (53), any load acting on the "translating side" of the actuation system is partly wasted into heat and partly converted by the lead screw into an equivalent moment on the "rotating side" of the system. As said above, inertia, elastic and friction forces may simultaneously act on the table, we have then that the <u>total</u> back-driving force as seen by the nut is:

$$N'_T(x) = -\frac{m_T}{2}\ddot{x} - F'_{qs}(x) = -\frac{m_T}{2}\ddot{x} - F'_0 - (K_r + K_{bl} + K_t)x \qquad \textbf{(54)}$$

The quasi-static contribution is taken with negative sign since in equation (38), F'_{qs} is the force to be supplied by the motor, opposed to the resultant of all quasi-static service loads.

In equation (54), m_T is the total mass to be moved (half of it by each table), including the inertial contribution of the pinion, shaft and other rotating elements of the anti-misalignment system.

If we indicate with I_{pT} the rotational inertia of these latter components and with D_P the primitive diameter of the pinion, and we assume a frictionless contact between the rack and the pinion, the equivalent mass of the anti-misalignment assembly can be calculated by the following formula[7]:

$$m_{pe} = I_{pT}\left(\frac{2}{D_P}\right)^2 \qquad \textbf{(55)}$$

---

[7] Equation (55) is obtained from the kinematic expression relating table displacement x with the pinion rotation θ, i.e. $\theta = \frac{2}{D_P}x$ and from the identity of work done on rotating and translating sides of the system in the absence of any loss, i.e. $m_{pe}\ddot{x}dx = I_{pT}\ddot{\theta}d\theta$

Hence $m_T = m_j + m_a + m_{pe}$. For a TCSG, $\boldsymbol{m_T = 44.9\ kg}$ and $\boldsymbol{m_{pe} = 0.3\ kg}$.

By equation (53), $N'_T(x)$ can be transformed back into an equivalent torque.

The basic equation of motion in case of auto-retraction for the rotary parts is then given by:

$$I_R\ddot{\varphi} = M + M'_b(x) + \eta'\frac{p}{2\pi}N'_T(x) \tag{56}$$

where $I_R = I_M + I_S$ is the total moment of inertia of the rotating parts. With its ***130 kgmm²*** the moment of inertia of the rotating parts of the motor is the most meaningful contribution (STÖGRA stepper motor based on type SM 87.2.18 [15]); I_S takes into account contributions from the screw shaft, the rollers, the inner ring of the bearing and the sleeve bushing (Figure 3-11): for a TCSG it is ***12.4 kgmm²***.

The additional term M is the ***detent torque*** applied by the stepper motor[8], i.e. the resistive moment the motor is applying when it is externally driven while not energized.

As in (46), the frictional moment generated by the bearing is proportional to the total force $N'_T(x)$:

$$M'_b(x) = -\mu N'_T(x)\frac{d}{2} \tag{57}$$

In equation (57), we implicitly assume that the direction of force N'_T is always the same of the motion (i.e. negative); in fact this is not granted, since during retraction the resultant might become positive: this simplification is necessary to treat analytically the problem.

As already seen, some terms linearly depend upon x, then separating the variable terms from the constant ones and replacing x with φ via relation (45), we obtain:

$$\begin{aligned} I_R\ddot{\varphi} = &-\left(\eta'\frac{p}{2\pi} + \mu\frac{d}{2}\right)\frac{m_T}{2}\frac{p}{2\pi}\ddot{\varphi} - \left[\left(\eta'\frac{p}{2\pi} - \mu\frac{d}{2}\right)\left(K_r + K_{bl} + K_t\right)\right]\frac{p}{2\pi}\varphi \\ &+ M + M_{b0} - \eta'\frac{p}{2\pi}F'_0 \end{aligned} \tag{58}$$

Regrouping and renaming different terms, we can finally write:

$$I_e\ddot{\varphi} + K_{eR}\varphi = T_{0e} \tag{59}$$

Where

$$I_e = I_M + I_S + \mu m_T\frac{dp}{8\pi} + \eta'\frac{m_T}{2}\left(\frac{p}{2\pi}\right)^2 \tag{60}$$

is the *equivalent* ***total moment of inertia*** (the last term is the contribution given by the translating mass),

$$K_{eR} = \left[\left(\eta' - \mu\frac{d\pi}{p}\right)K_T\right]\left(\frac{p}{2\pi}\right)^2 \tag{61}$$

is the ***equivalent torsional stiffness*** and

[8] The detent torque, on top of mechanical frictions generated by the motor bearings, mostly depends on the resistive forces created by the permanently magnetized components of the hybrid stepper motor. The higher the pull-in torque (i.e. nominal rated torque), the larger these forces.

$$T_{0e}(M) = -\eta' \frac{p}{2\pi} F_0' + M + M_{b0} \quad \textbf{(62)}$$

is the ***equivalent static torque***.

It is immediate to realize that (59) is the governing equation of a harmonic system with one degree of freedom, whose solution is well known [14].

For practical reasons, it is more convenient to express equation (59) in terms of the linear displacement *x* (by multiplying both parts by *2π/p* and making use of equation (39)):

$$m_e \ddot{x} + K_e x = F_{0e} \quad \textbf{(63)}$$

Where

$$m_e = I_e \left(\frac{2\pi}{p}\right)^2 = \left(I_S + I_M + \mu m_T \frac{dp}{8\pi}\right)\left(\frac{2\pi}{p}\right)^2 + \eta' \frac{m_T}{2} \quad \textbf{(64)}$$

is the ***equivalent mass***,

$$K_e = K_{eR}\left(\frac{2\pi}{p}\right)^2 = \left(\eta' - \mu \frac{d\pi}{p}\right) K_T \quad \textbf{(65)}$$

is the ***equivalent spring stiffness*** and

$$F_{0e}(M) = T_{0e}(M)\frac{2\pi}{p} = \left(-\eta' \frac{p}{2\pi} F_0' + M + M_{b0}\right)\frac{2\pi}{p} \quad \textbf{(66)}$$

is the ***equivalent static force*** (depending on the motor detent torque). Assuming a detent torque of *100 Nmm*, for a TCSG F_{0e} is ***212 N***. A larger screw lead implies smaller static forces.

It is interesting to note that, by far, the largest contribution to the *equivalent mass* is given by the rotating parts (and in particular by the rotor of the stepper motor) rather than by the actual translating mass: for instance for a TCSG collimator, with ***η' = 0.5***, we have $\boldsymbol{m_e = 1417\ kg}$, the contribution from the translating mass being **11.2 *kg,*** from the screw assembly ***121.9 kg*** and from the motor ***1283 kg***! This is mainly deriving from the multiplying effect given by the small lead per revolution ratio.

On the other hand, the equivalent stiffness is reduced by the combined effect of bearing friction and indirect efficiency, in fact, for the same TCSG with stiff return springs, $\boldsymbol{K_e}$ **= 10.9** ***N/mm*** while $\boldsymbol{K_T}$ **= 24.2** ***N/mm***. As one might expect, for η'= 1 and μ = 0, $K_e = K_T$.

Indicating with

$$\delta_e(M) = \frac{F_{0e}(M)}{K_e} \quad \textbf{(67)}$$

the *equivalent static deflection* and effectuating the change of variables $x(t) = z(t) + \delta_e$, equation (63) can be reduced to a homogeneous one.

Boundary and initial conditions are given by $x(0) = c$ and $\dot{x}(0) = 0$, where *c* indicates the jaw position at the instant when auto-retraction is required (typically the jaw working position). Solution is then given by:

$$x_h(t) = \delta_e + (c - \delta_e)\cos(\omega_e t) \quad \textbf{(68)}$$

The circular frequency of the system ω_e is given by:

$$\omega_e = \sqrt{\frac{K_e}{m_e}} \quad \textbf{(69)}$$

Minimum of function (68) is found at

$$\tau_{\min} = \frac{\pi}{\omega_e} \tag{70}$$

For a TCSG with stiff springs, ω_e **= 2.78** ***rad/s*** (**0.44** ***Hz***) and τ_{min} **= 1.13** *s*; the value of *x* minimum is:

$$x_{hMin} = 2\delta_e - c = 2\frac{F_{0e}(M)}{K_e} - c \tag{71}$$

We observe that x_{hMin} is smaller (i.e. auto-retraction is greater) when the equivalent stiffness K_e is high and the static force F_{0e} is low, which, in turns, occurs if detent torque is small. Also, the larger *c*, the smaller x_{hMin}, i.e., all other parameters being equal, auto-retraction is greater when the jaw is closer to its full-in position.

Obviously, equation (68) has physical meaning only if $x_{hMin} \le c$ (if not, this would mean the jaw is moving towards the beam, i.e. auto-retraction is impossible) and $x_{hMin} \ge 0$ (if not, this means the table has been blocked at x=0 by the outer stop). Additionally, due to the reversal of friction forces, the table cannot change the direction of its motion once it has attained zero velocity at $t = \tau_{min}$, then it stops as if the system were critically damped.

Mathematically we can express all preceding conditions via the following equation:

$$x(t) = \begin{cases} x_h(t) & if \quad 0 \le t \le \tau_{\min} \wedge 0 \le x_{hMin} \le c \\ x_{hMin} & if \quad t > \tau_{\min} \wedge x_{hMin} \ge 0 \\ c & if \quad x_{hMin} > c \\ 0 & otherwise \end{cases} \tag{72}$$

Figure 4-1 shows the backward stroke plotted against time, from the initial nominal position c = 28.5 *mm*, for four different values of the motor detent torque *M*. The collimator orientation angle is β=90° (i.e. weight force tends to move the jaw in), stiff return springs are considered.

It is worth noting the considerable influence of detent torque on the auto-retraction: at 80 *Nmm* the full backward travel is still possible but already at 120 *Nmm*, the return stroke is limited to ~6 mm only and at 140 Nmm, auto-retraction is zero for this configuration.

In Figure 4-2 velocity of the jaw during auto-retraction is shown; this plot is particularly useful to estimate the impact velocity of the mobile table on the outer stop in case of full stroke and to evaluate the maximum rotational speed of the roller screw, which is a relevant parameter to establish its expected lifetime.

At *80 Nmm*, the maximum speed is *41.2 mm/s*, whereas the impact speed is *15.9 mm/s*.

The highest theoretical speeds may be achieved in case the detent torque is zero and the collimator is horizontal with stiff springs (highest available drive-back forces): in this case the maximum speed would be *148.4 mm/s* and the impact speed *139.3 mm/s*. These values are sufficiently small to make unnecessary the adoption of shock-absorbing systems at the full-out stop.

The maximum rotational speed of the screw in the latter case would be 4452 RPM which is some percentages of the critical rotational speed, which is found above 100000 RPM [3].

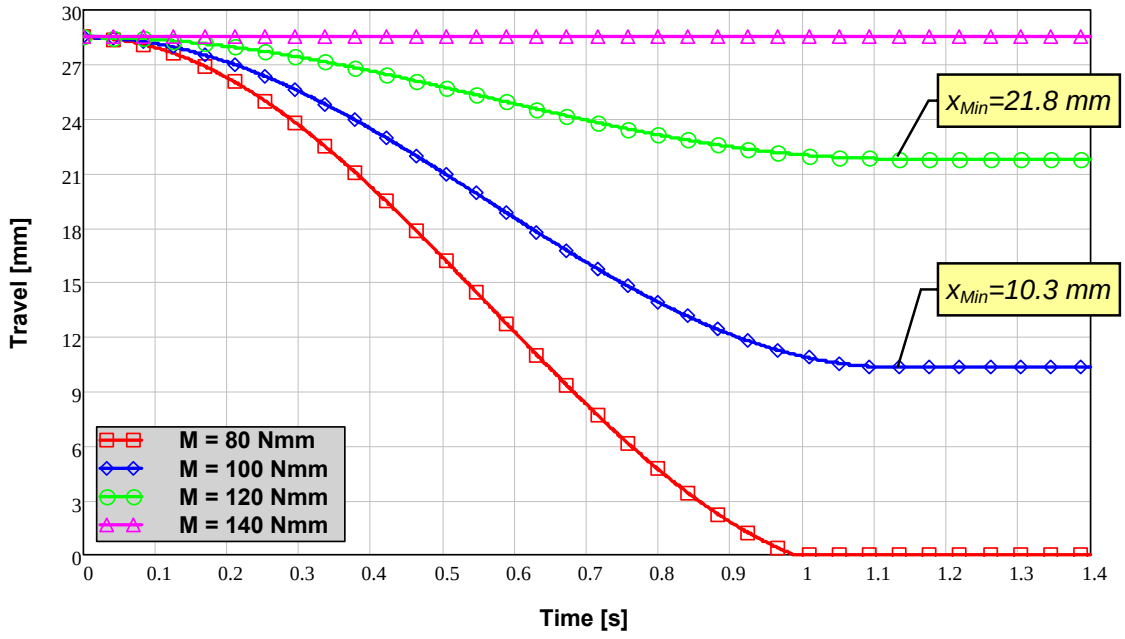

Figure 4-1 Backward stroke from nomimal position as a function of time for different values of motor detent torque for TCSG collimator, orientation 90°, stiff springs

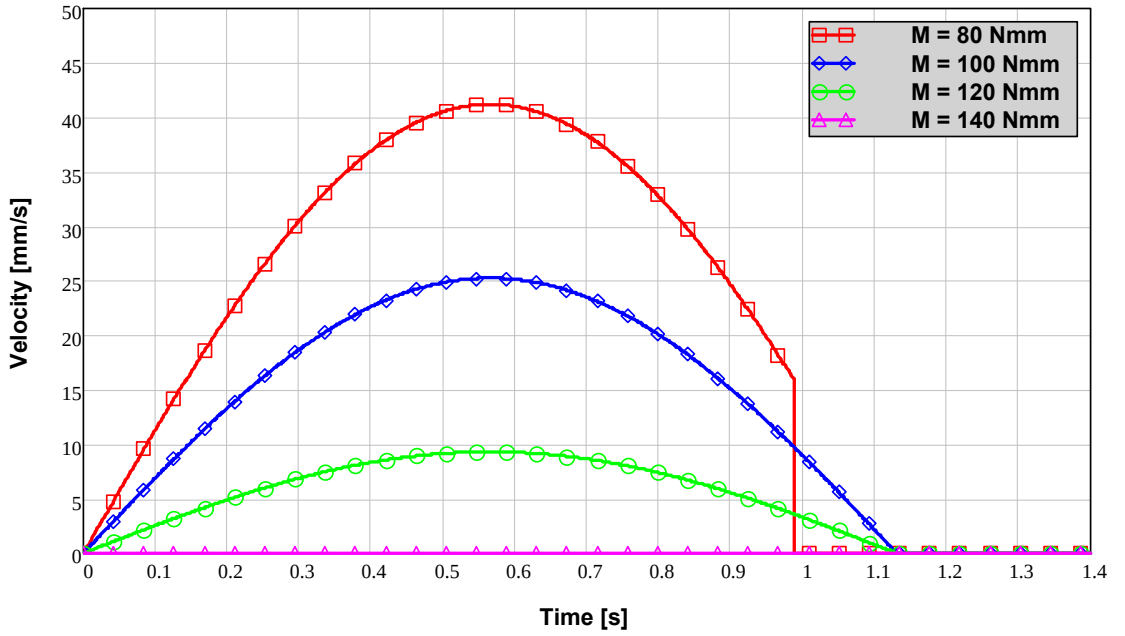

Figure 4-2 Mobile table velocity (absolute value) during auto-retraction for different values of detent torque (initial position c_{nom})

5 CONCLUSIONS

In this note the design of the actuation system for the LHC Collimators (Phase I) is presented. The various loads acting on the system are examined in view of determining the motor torque required to move the jaw in and out. An analytical method to anticipate the system behavior when auto-retraction is requested is worked out and presented in detail. This analysis allowed to identify the parameters that influence the auto-retraction behavior and to quantify their effect: we have found that detent torque of the stepper motor is of paramount importance and must be carefully checked if auto-retraction is aimed. Detailed results for each collimator configuration, along with specific design features, are given in the appendix.

6 REFERENCE DOCUMENTS

[1] LHC Design Report, Vol.I, Chapter 18, *Beam Cleaning and Collimation System*, 2004.

[2] A. Bertarelli et al., *The Mechanical Design for the LHC Collimators*, Proceedings EPAC 04, 2004

[3] SKF Linear motion, *Roller screw manual*, http://www.linearmotion.skf.com

[4] http://www.lubodry-productions.com

[5] http://www.santovac.com/techdata/sv5gbtechdata.htm

[6] R. Losito, *Private Communications*, 2005

[7] COMVAT AG, *Bellows datasheet Product-No. 127588*

[8] MEWASA AG, *Bellows datasheet OF-04-5638*.

[9] R. de Morais Amaral et al., *Tests of a Graphite-based Dry Lubricant for Phase I Collimators Linear Bearings*, EDMS 1031803, 2009

[10] SKF Linear motion, *Precision Rail Guides Catalogue*, www.linearmotion.skf.com.

[11] Schneeberger AG, *Linear Bearings and Recirculating Units Catalogue*, www.schneeberger.com.

[12] Feuerherdt GmbH, *General catalogue, Contact Strips*, *8104.00.02*, www.shielding-online.com

[13] P. Smas, A. Dallocchio, A. Bertarelli, *Finite-element analysis of the RF end transitions for the LHC Collimators*, EDMS 886329, 2007.

[14] Thomson W.T., Dahleh M.D., *Theory of vibration with applications*, Fifth edition, Prentice Hall, New Jersey, 1998.

[15] Stögra, *Stepper motors catalogue 2007*, http://www.stoegra.de/pdf/sm_katalog_1106_e.pdf

[16] Verein Deutsche Ingenieure Norm,*VDI 2230 – Systematic calculation of high duty bolted joints*, 2003

[17] J.E. Shigley et al., *Mechanical Engineering Design*, 7th edition, McGraw-Hill, New York, 2007.

[18] General catalog SKF, *Catalog 6000 EN*, November 2005.

[19] Gutekunst Federn, *Spring catalog*, www.gutekunst-co.com

[20] LHC documentations, *Table collimator TCS translation screw support*, Drawing LHCTCS__0083.

7 APPENDIX

In the following paragraphs quantitative results are reported for different collimator types in various configurations. Most meaningful data are the required motor torque to drive in the jaw assembly and, when applicable, the system behavior in case of auto-retraction. It is important to bear in mind that these values were obtained from an analytical model in which, to make it exploitable, a number of simplifications and omissions were done; besides, most input data (e.g. stiffness of springs, bellows characteristics, weights and inertias etc.) are based on figures obtained from nominal or ideal configurations, and are inevitably affected by a certain dispersion. Therefore, all results should be treated with due caution and, when used for system qualification, adjusted by adequate safety coefficients.

7.1 Secondary Collimator (TCSG)

Secondary collimators are the most widely used and exhibit all possible orientations. As explained later, two different return springs may be mounted depending on azimuth β; in this note we assume stiff springs are used when $\beta \geq 0^o$ and soft springs otherwise: results are shown accordingly (for the horizontal orientation, results for both spring types are presented). Anyway, different configurations are possible depending on production decisions at final assembly. It will be seen that stiff springs may be chosen for any TCSG orientation, improving auto-retraction in all cases.

7.1.1 Weight and equivalent masses

The masses, real or equivalent, of the jaw assembly and of the other mobile parts necessary to compute the weight force and the total inertia of the system are given in Table 7-1. For details about the meaning of each term, see equation (55) and following ones.

Assembly		***Mass [kg]***
m_j	*Jaw Assembly (Carbon/Carbon)*	*33.5*
m_a	*Axle and mobile table components*	*11.4*
m_{pe}	*Rack and pinion (equivalent)*	*0.3*
m_M	*Motor rotating parts (equivalent)*	*1283.0*
m_S	*Screw and other rotating parts (equivalent)*	*121.9*
m_e	*Total equivalent mass (including friction term)*	*1417.3*

Table 7-1 Masses of the mobile parts for a TCSG

7.1.2 Return spring force

Two alternative types of springs are foreseen for a TCSG, depending on the collimator orientation and jaw weight: a stiff spring is recommended to ease the auto-retraction of jaws against the weight ($\beta \geq 0^o$) and a soft spring may be used in the other cases. Spring data are given in Table 7-2. The mounted spring length (full-out position) is L_{ro}=120 *mm*. Maximum travel is 35 *mm*.

Spring type	Mean diameter D [mm]	Wire diameter d [mm]	Free length L_o [mm]	Min. admissible length L_n [N/mm]	Spring ratio K_r [N/mm]
VD-377 (stiff)	50	6.3	175	76.56	12.97
VD-347 (soft)	50	5	195	63.13	5.15

Table 7-2 Spring data

7.1.3 Bellows force

Two bellows types from different suppliers are alternatively used for TCSG collimator. Bellows data are given in Table 7-3.

Type	Nominal lateral spring rate K_{bn} [N/mm]	Lateral admissible stroke c_{bl} [mm]	Lateral maximum vacuum force $F_{pl}(c_{bl})$ [N]	Straight bellows position L_{bn} [mm]
1 (COMVAT)	0.72	20	157.6	18.5
2 (MEWASA)	0.1	20	210	

Table 7-3 Bellows data

Bellows force plot is shown in

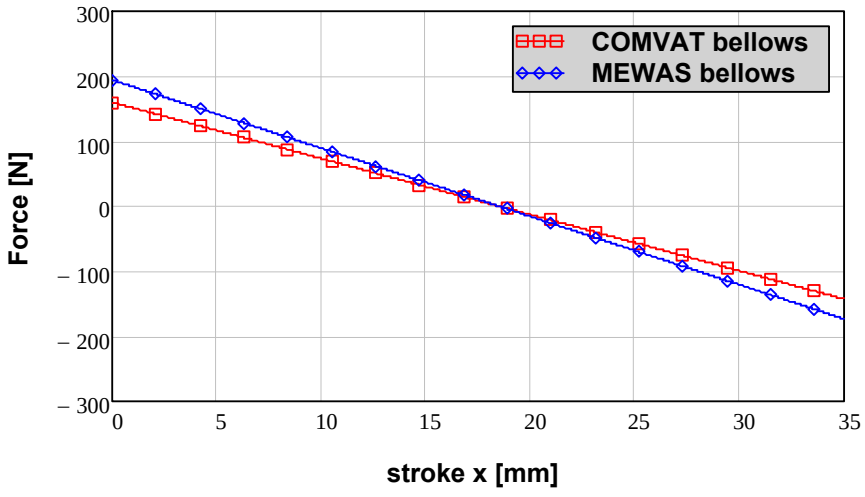

Figure 7-1. The force values for full-out F_{bo} and full-in F_{bc} jaw positions of both types are indicated. Results presented in this note correspond to bellows type 2.

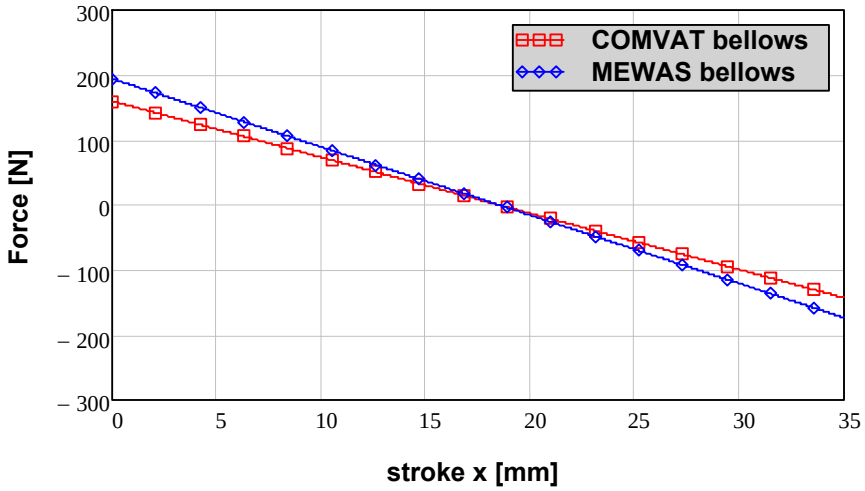

Figure 7-1 Bellows force as a function of stroke

7.1.4 Linear bearing friction force

As described in 3.1.4, for TCSG, linear bearings with crossed-roller cages, made of corrosion resistant materials, are used. Relevant data derived from suppliers catalogs [9] [11], are given in Table 7-4.

Number of Rollers	Permissible load per roller C [N]	Allowable roller preload p_r [%]	Length between preload screws L_1 [mm]	Roller pitch t [mm]	Number of set-screws per rail n_{vs}	Number of active rollers per screw n_r
18	410	2 - 20	100	9	2	11

Table 7-4 Linear bearing data - type SKF LWR6 (Source SKF and Schneeberger)

Main parameters allowing to compute the maximum expected friction force are presented in Table 7-5.

Max preload (per screw) F_{vs} [N]	Max preload (per linear bearing) F_{rtMax} [N]	Actual preload (per linear bearing) F_{lb} [N]	Max Friction Coefficient η_t	Friction force (per table) F_{ft} [N]
902	1804	1360	0.003	8.8

Table 7-5 Calculated quantities for the linear bearing - type SKF LWR6

7.1.5 Friction force due to longitudinal RF contacts

As detailed in paragraph 3.1.5, the estimated friction force per jaw assembly is computed in the hypothesis of 1 mm alignment error, leading to a force of *60* N (see Table 7-6).

Friction coefficient	Misalignment error parameter	RF Contact Force (per rail)	RF Contact Friction Force (per table)

μ_{rf}	*err* [mm]	F_{rf} [N]	F_{fr} [N]
0.6	1	199.6	59.8

Table 7-6 RF contact friction force

7.1.6 Quasi-static forces

The plots of the total drive-in force $F_{qs}(x)$ and drive-back force $F'_{qs}(x)$ which the motor must supply, calculated in compliance with equations (36) and (38), are presented in Figure 7-2 and in Figure 7-3. The highest quasi-static force (in magnitude) required to drive the TCSG jaw assembly to the full-in position is found at $\beta = 0^o$ (when stiff springs are used) and amounts to *1428* N. This value is important to define the minimum required motor torque. Needless to say, if stiff springs are used also for negative orientations (i.e. -45º and -90º), a higher maximum force is to be expected.

The minimum available back-driving force equals *117* N and is found at $x = 0$ for $\beta = 0^o$ using soft springs. It is interesting to see that drive-back force is always positive for any collimator configuration, meaning that the motor is always pushing in (i.e. braking) when driving the jaw assembly back, in other words the system is always tending to self-retract.

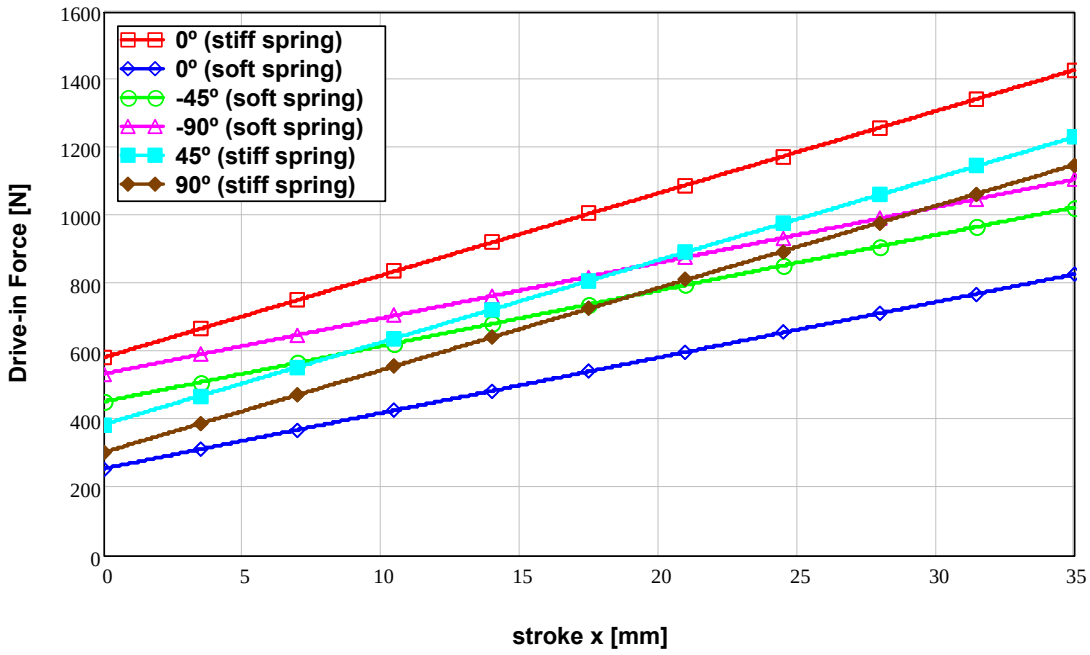

Figure 7-2 TCSG: Total quasi-static force required to drive in the jaw in various configurations

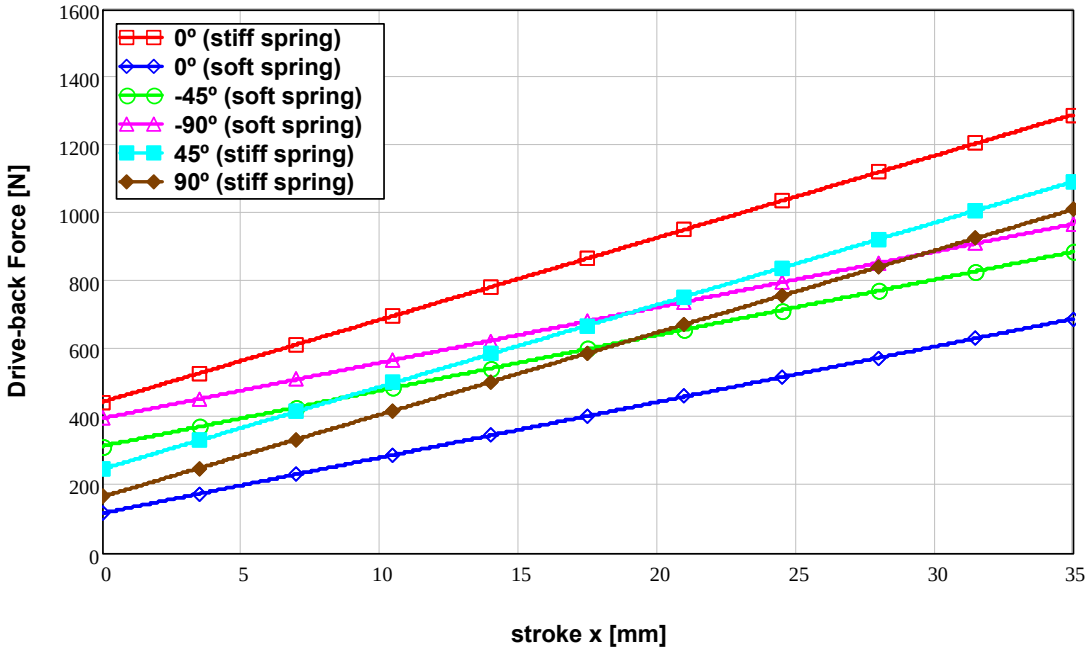

Figure 7-3 TCSG: Quasi-static back-driving force in various configurations

7.1.7 Ball Bearing friction

The TCSG roller screw is supported on its shaft end by a deep groove ball bearing (20x42x12 SKF 6004) (see Figure 3-11). Relevant data to compute the friction moment induced by this bearing (according to equations (45) and (46)) are given in Table 7-7 [13].

Inner diameter d [mm]	Outer diameter D [mm]	Width B [mm]	Outer diameter of internal ring d_1 [mm]	Basic static load ratings C_0 [kN]	Friction coefficient μ
20	42	12	27.2	5.0	0.0015

Table 7-7 Deep groove ball bearing, single row 20x42x12 SKF 6004 data

7.1.8 Roller screw data

Data for the roller screw SVF 12x2-R2 90/135 G1 Z NOPWR [3] are given in Table 7-8. Friction coefficient has been measured by the supplier in an extensive experimental campaign, taking into account the effect of graphite coating (Lubodry G) and radiation-hard grease.

Nominal diameter d_0 [mm]	Lead p [mm]	Length L_s [mm]	Friction coefficient μ_s	Roller screw shaft inertia I_s [kgmm^2/m]	Rollers inertia I_{ns} [kgmm^2]
12	2	135	0.02651	14.2	0.1

Table 7-8 Roller screw SVF 12x2-R2 90/135 G1 Z NOPWR data

7.1.9 Direct and indirect efficiency

Direct efficiency, practical efficiency and indirect efficiency are computed by means of eqs. (41), (42) and (43) using data provided in Table 7-8. For a TCSG we have obtained

$$\eta = 0.667$$

$$\eta_p = 0.6$$

$$\eta' = 0.5$$

7.1.10 Quasi-static drive-in and drive-back torque

The torque $T_{qs}(x)$ which the motor has to supply to drive in the jaw is presented, as a function of stroke, in Figure 7-4 for various TCSG configurations. The highest torque (**0.78 Nm**) is required to drive in a horizontal TCSG featuring stiff springs. As said above if stiff springs are used also for negative orientations, higher torques will be required.

For the jaw retraction three scenarios are possible: if everything is working correctly, the actuation is overseen by the two motors which must always supply a certain braking torque $T'_{qs}(x)$, as shown in Figure 7-5, since the torque generated by the mechanical system is always trying to push back the system (bearing in mind that in this case the detent torque does not appear in equation (51)).

If both motors fail to work (e.g. no electric power), we want to know the net torque, provided by the mechanical system (opposed in sign to $T'_{qs}(x)$), which is available to drive back the jaw taking into account the motor detent torque. In this case, because of the detent torque effect, the torque which is actually available may be positive, i.e. auto-retraction cannot be started in quasi-static condition. In Figure 7-6, the case for a detent torque of 0.08 *Nm* is shown.

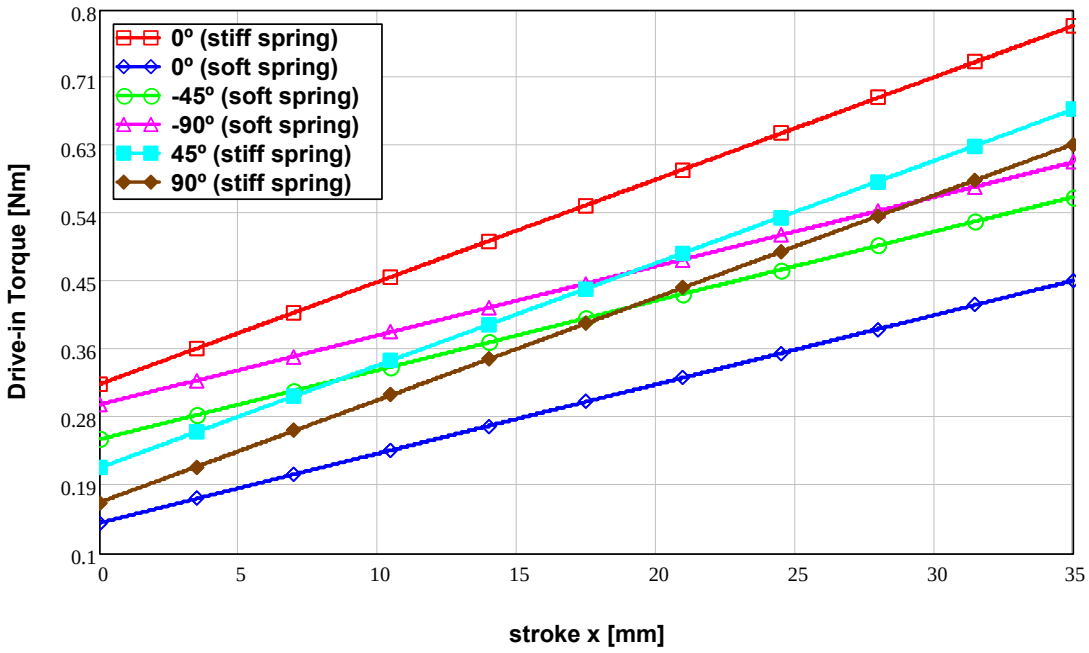

Figure 7-4 TCSG: required motor torque *T(x)* as a function of stroke

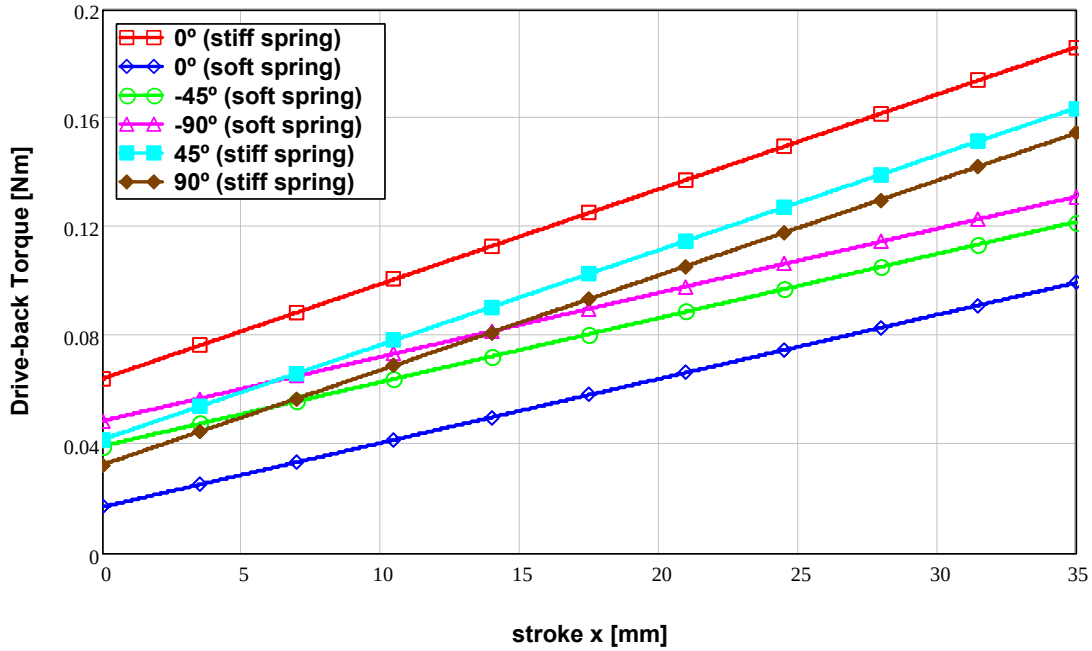

Figure 7-5 TCSG: Quasi-static braking torque to be supplied by the motor during jaw back-driving

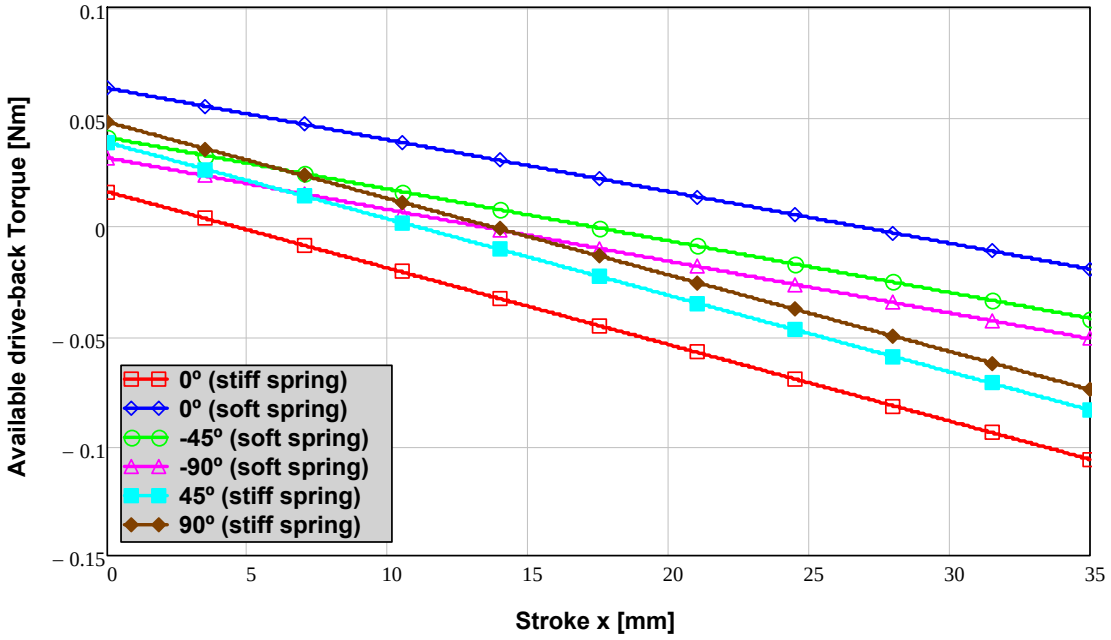

Figure 7-6 TCSG: Available quasi-static torque for auto-retraction with a motor detent torque of 80 Nmm

Finally, if we assume that one motor only is working and the other is idle, the other motor might have to provide positive or negative torque (i.e. driving or braking) depending on the detent torque which the failed motor is generating.

7.1.11 Dynamic analysis of auto-retraction

In this paragraph the expected behaviour in case of auto-retraction is presented for different collimator orientations

7.1.11.1 Horizontal TCSG (0°)

For the horizontal configuration we have studied auto-retraction both in case of stiff and of soft return springs. Figure 7-7 shows the expected jaw back-travel as a function of motor detent torque and of jaw initial position when stiff springs are mounted. Figure 7-8 shows the same plot in case of soft springs. In each plot the axis of abscissas gives the final position, so entering for instance in Figure 7-7 with a detent torque of 140 *Nmm*, we find that the expected return travel is roughly 26.5 *mm* if the initial position was 35 *mm*, the travel is reduced to 16.5 *mm* if starting from 30 *mm* and so on. The auto-retraction is complete, when the stroke is equal to the initial position. We can clearly see that the use of stiff springs allows a much better retraction compared to soft springs: in particular for the same torque of 140 *Nmm*, self-retraction is impossible from any initial position with soft springs while it is to a large extent feasible for the other case.

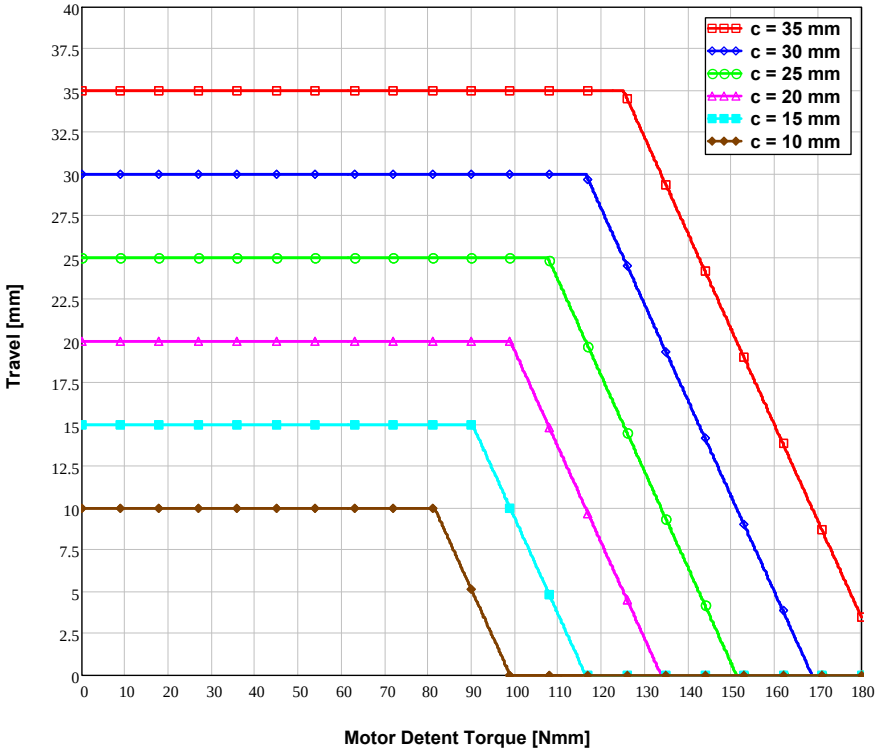

Figure 7-7: Dynamic reverse travel vs. detent torque with various initial positions (stiff springs, 0°)

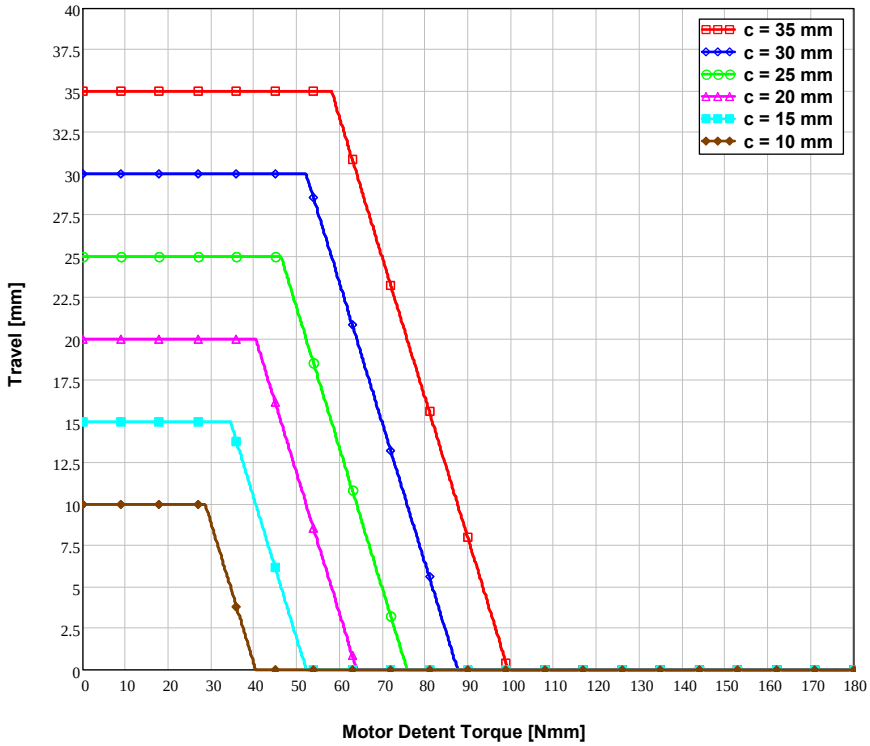

Figure 7-8: Dynamic reverse travel vs. detent torque with various initial positions (soft springs, 0º)

7.1.11.2 Skew TCSG (-45º)

Same plots as for horizontal collimator are shown also for a jaw at -45º. Although for such a configuration soft springs are usually envisaged, results for stiff springs are also given (Figure 7-9 and Figure 7-10).

7.1.11.3 Skew TCSG (+45º)

In this case stiff springs only are foreseen. Results are given in Figure 7-11.

7.1.11.4 Vertical TCSG (-90º)

Results the jaw of a vertical collimator which tends to move backwards (-90º) are given in Figure 7-12. Mounted springs are the soft ones.

7.1.11.5 Vertical TCSG (90º)

For the jaw of a vertical collimator which tends to move towards the beam axis, stiff springs are used. Results are given in Figure 7-13.

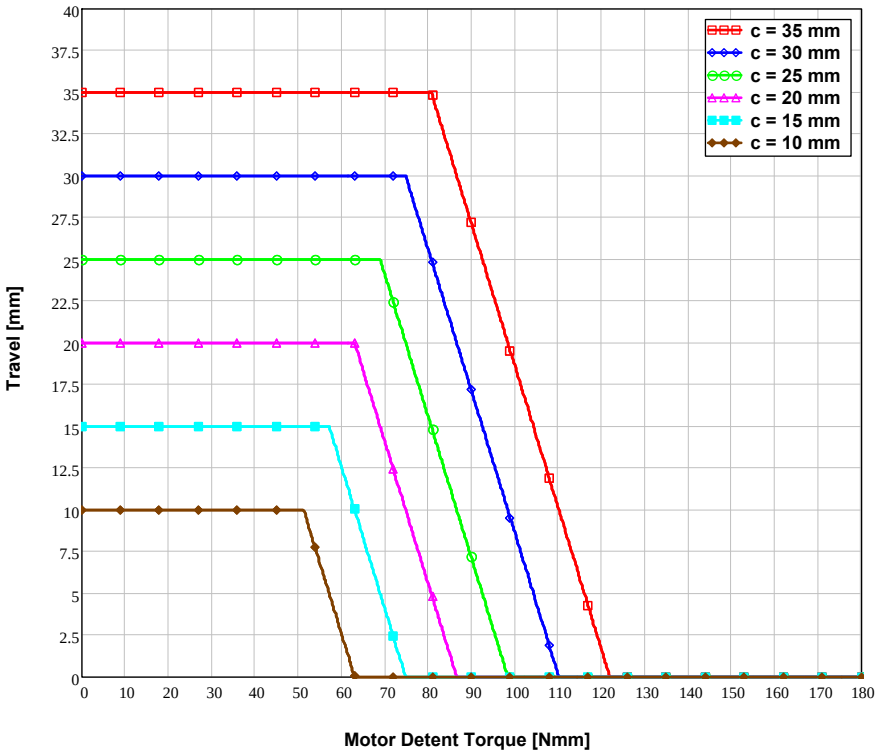

Figure 7-9: Dynamic reverse travel vs. Detent Torque with various initial positions (soft springs, -45º)

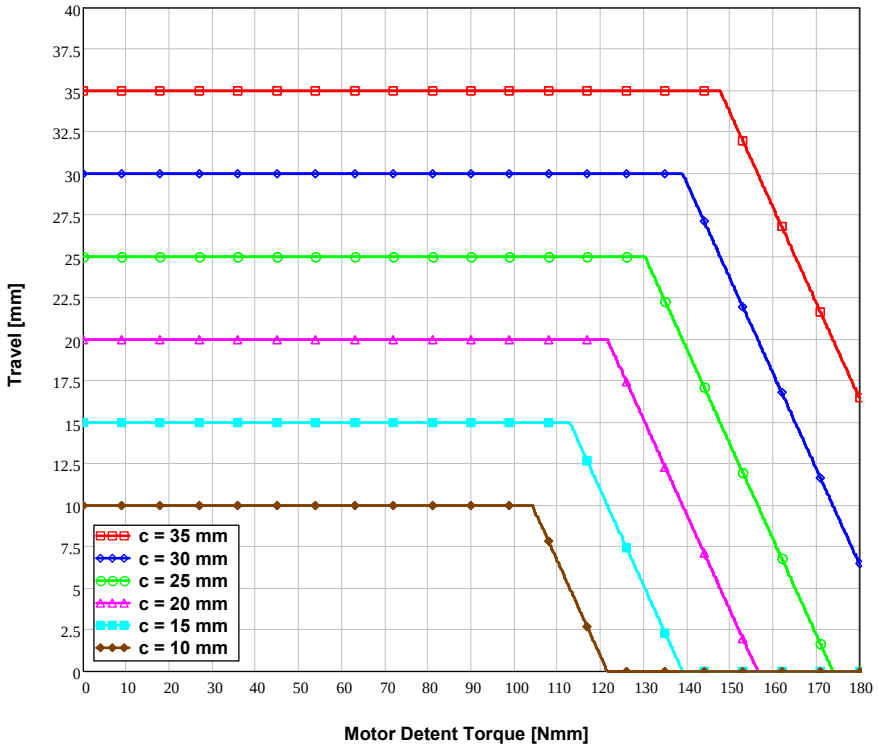

Figure 7-10: Dynamic reverse travel vs. detent torque with various initial positions (stiff springs, -45º)

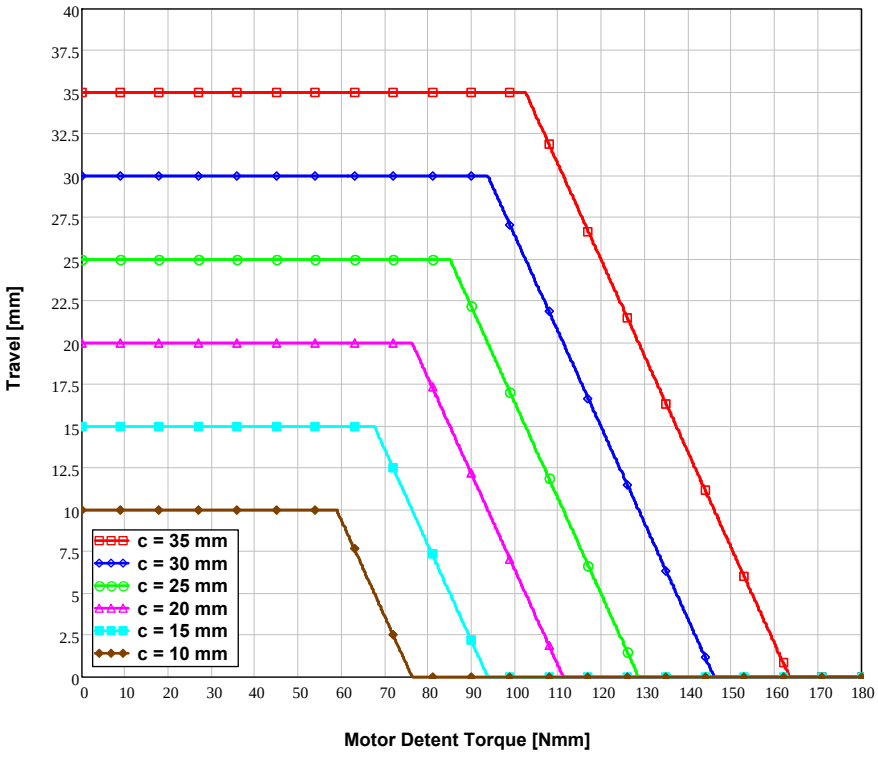

Figure 7-11: Dynamic reverse travel vs. detent torque with various initial positions (stiff springs, +45º)

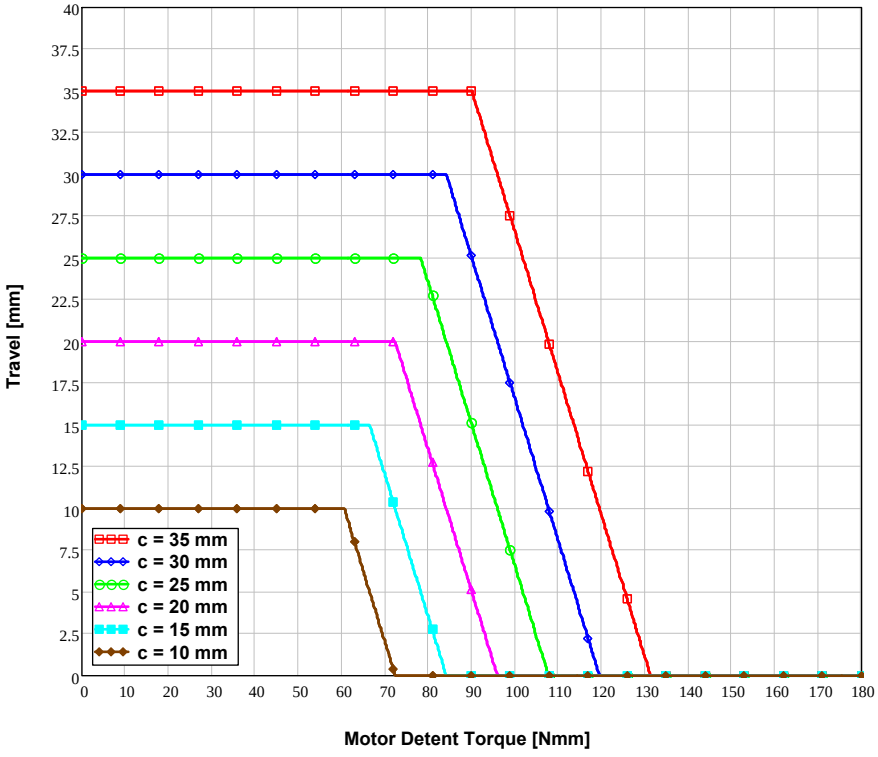

Figure 7-12: Dynamic reverse travel vs. Detent Torque with various initial positions (soft springs, -90º)

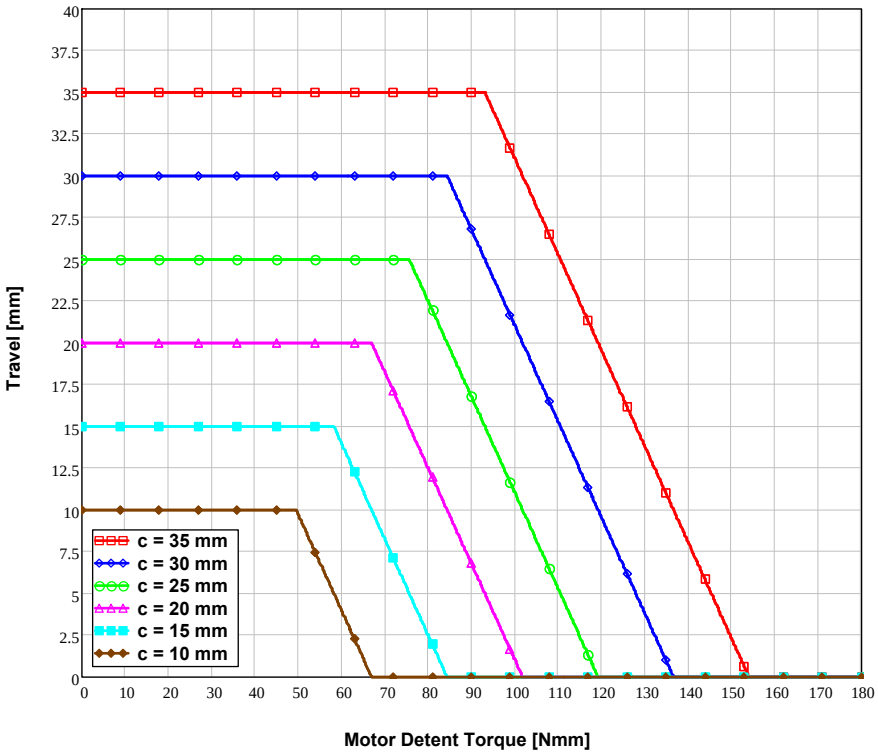

Figure 7-13: Dynamic reverse travel vs. Detent Torque with various initial positions (stiff springs, +90º)

7.2 Primary Collimators (TCP)

Primary collimators only differ from TCSG in the C/C jaw, which has slightly different shape to reduce the active collimation length. The overall assembly weight is very little affected by this aspect; therefore the results for secondary collimators can be retained for this version as well.

7.3 Tertiary collimators type A (TCTA)

Tertiary collimators are mainly used to protect the Superconducting Triplets in the experimental insertions from the beam halo generated by the secondary collimators. There are two types of Tertiary Collimators (A or B) according to the fact that one or both beams are passing through the collimators tank. TCTA are derived from the TCSG design: they share the same tank, the same actuation system and part of the jaw assembly. The main difference is in the jaw itself, which for the TCT is made of 5 blocs of tungsten alloy (Inermet 180), each one *200* mm long, embedded in a Cu-OFE support. Only two orientations are envisaged for TCTA: horizontal and vertical. The jaw assembly of a TCTA is shown in Figure 7-14.

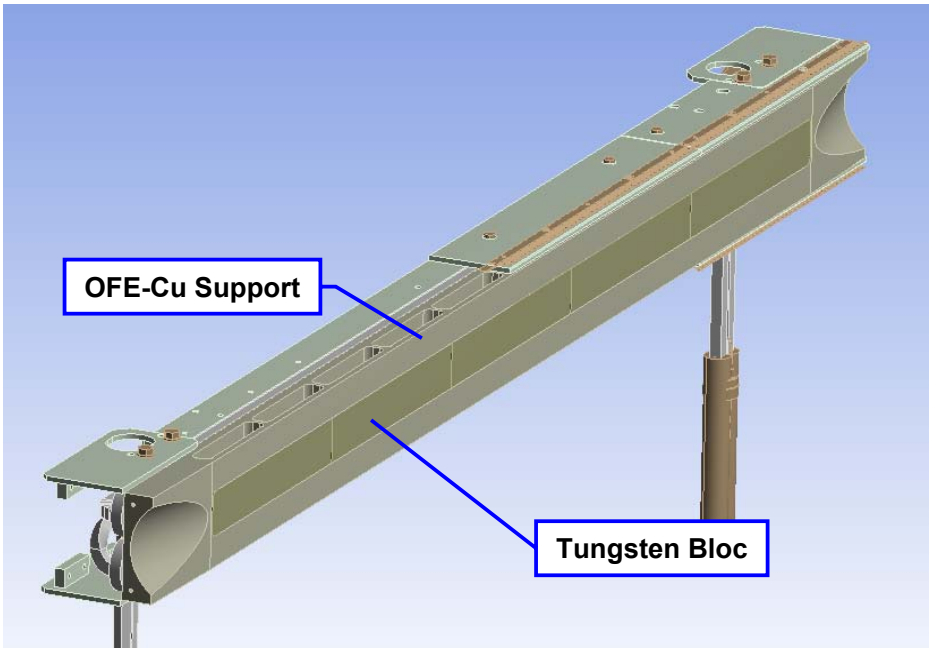

Figure 7-14 Jaw assembly of a TCTA

7.3.1 Weight

The weight Q_j of TCTA jaw assembly is **448** ***N***. Weight of other mobile parts is given in Table 7-1.

7.3.2 Quasi-static forces

Plots of the quasi-static forces to drive in and back the jaw assembly are given in Figure 7-15 and Figure 7-16. Curves at 0º are the same as for TCSG since weight plays no role in quasi-static motion at this orientation.

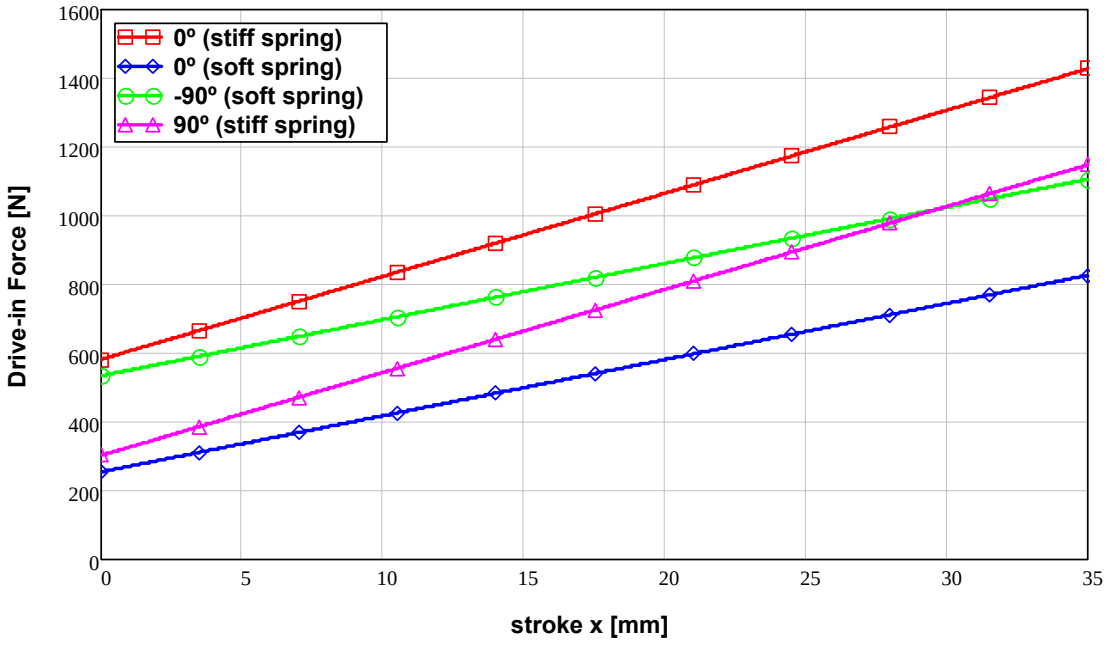

Figure 7-15 TCTA: Total quasi-static force required to drive in the jaw in various configurations

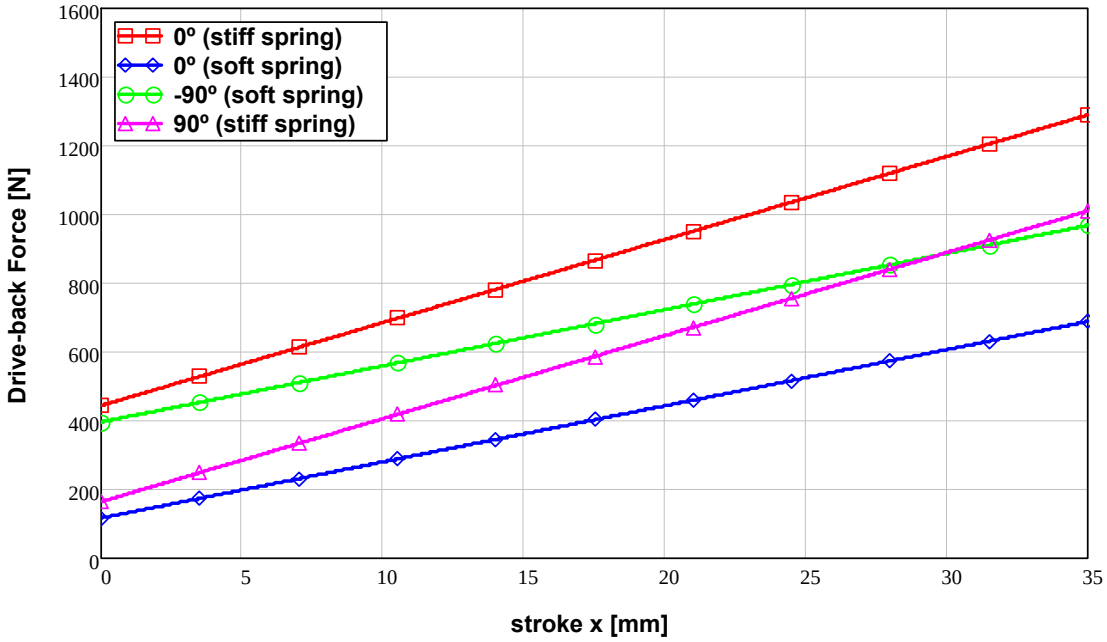

Figure 7-16 TCTA: Quasi-static back-driving force in various configurations

7.3.3 Quasi-static drive-in and drive-back torque

Figure 7-17 shows the torque required to drive in a TCTA jaw as a function of stroke in various configurations. In Figure 7-18 quasi-static back motion is described: negative torque indicates that the motor is braking to counteract the mechanical force pushing the jaw backwards. In case of motor failure, its detent torque must be added: available auto-retraction torque is exemplified in Figure 7-19. It can be seen that below certain jaw positions x auto-retraction can never be started.

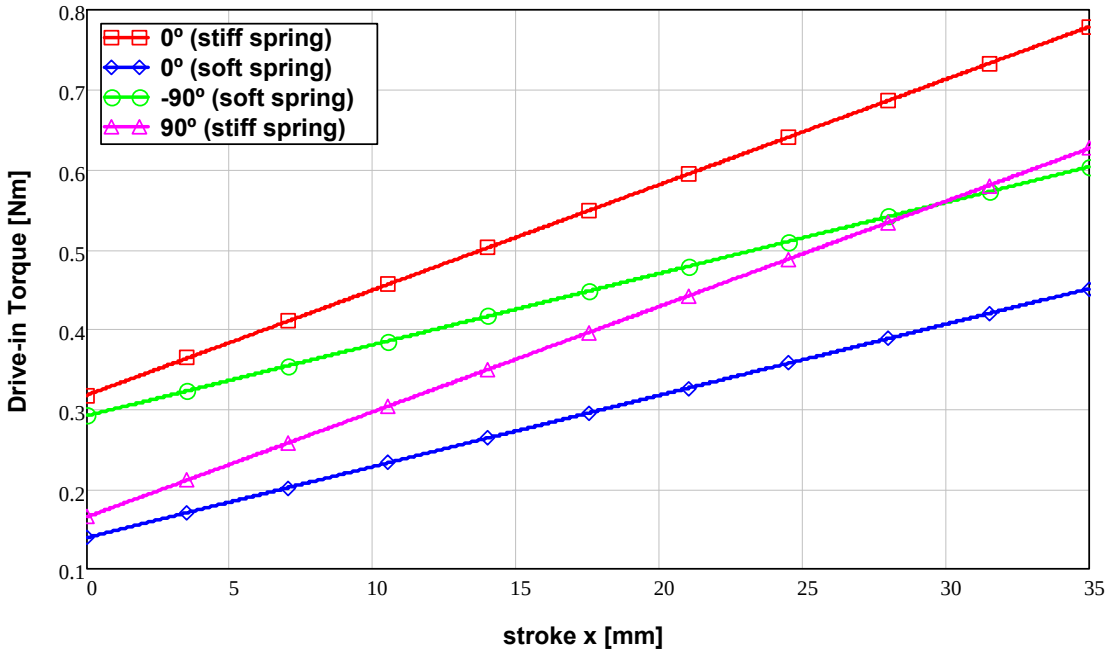

Figure 7-17 TCTA: Quasi-static motor torque $T_{qs}(x)$ required to drive-in the jaw as a function of stroke

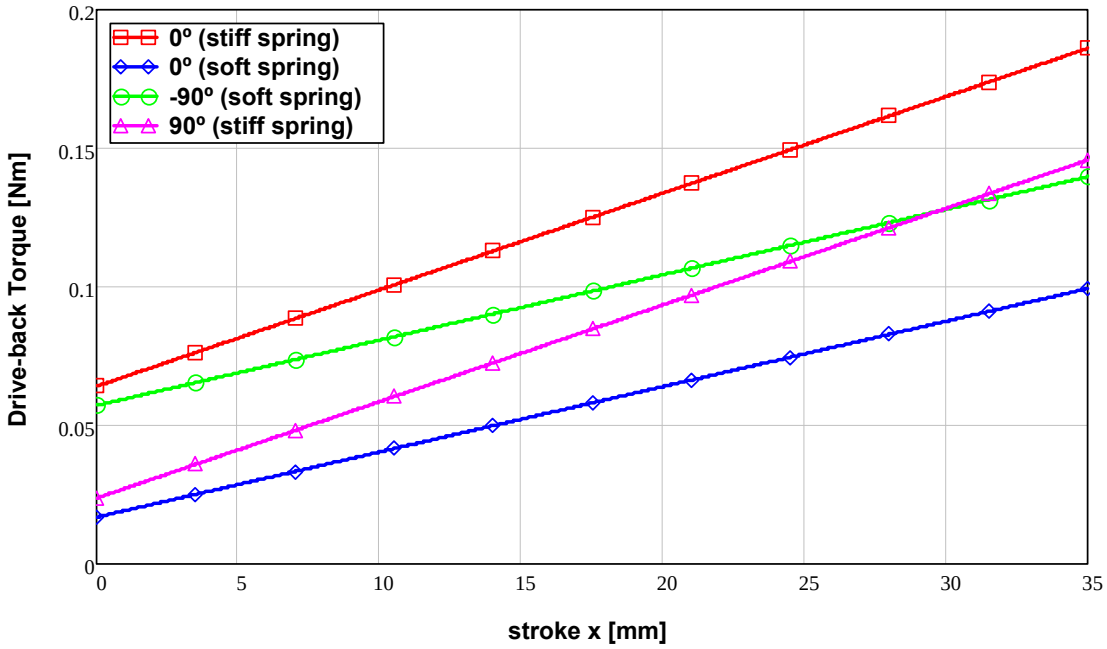

Figure 7-18 TCTA: Quasi-static braking torque $T'_{qs}(x)$ to be supplied by the motor during back-driving

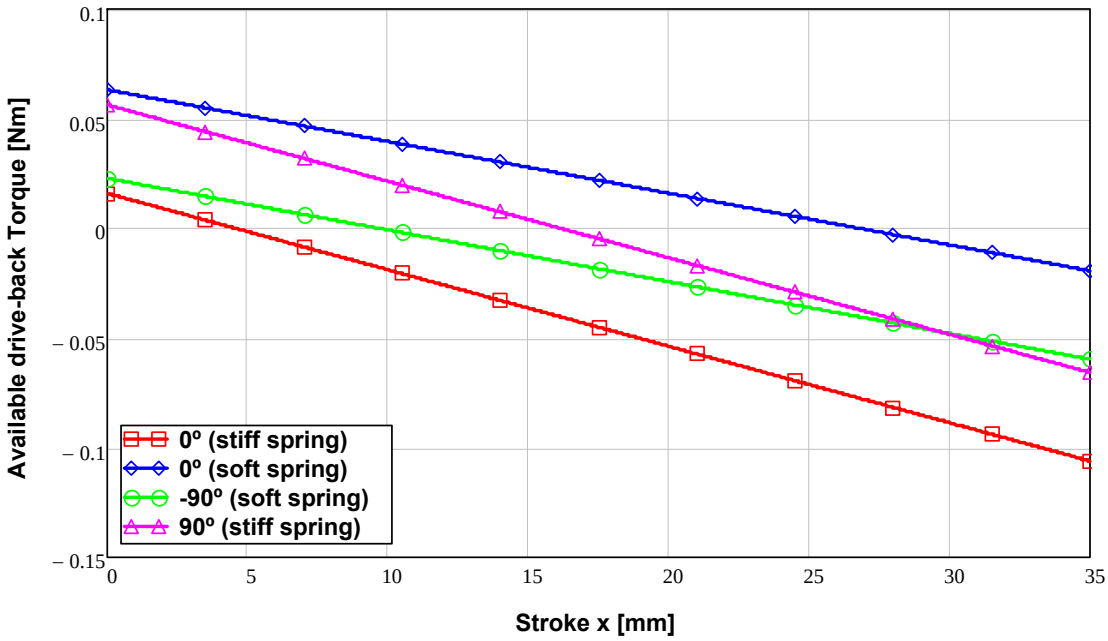

Figure 7-19 Available quasi-static torque for auto-retraction with a motor detent torque of 80 *Nmm*

7.3.4 Dynamic analysis of auto-retration

As said above only two orientations are envisaged for TCTA, horizontal and vertical.

7.3.4.1 *Horizontal TCTA (0°) – Stiff and soft springs*

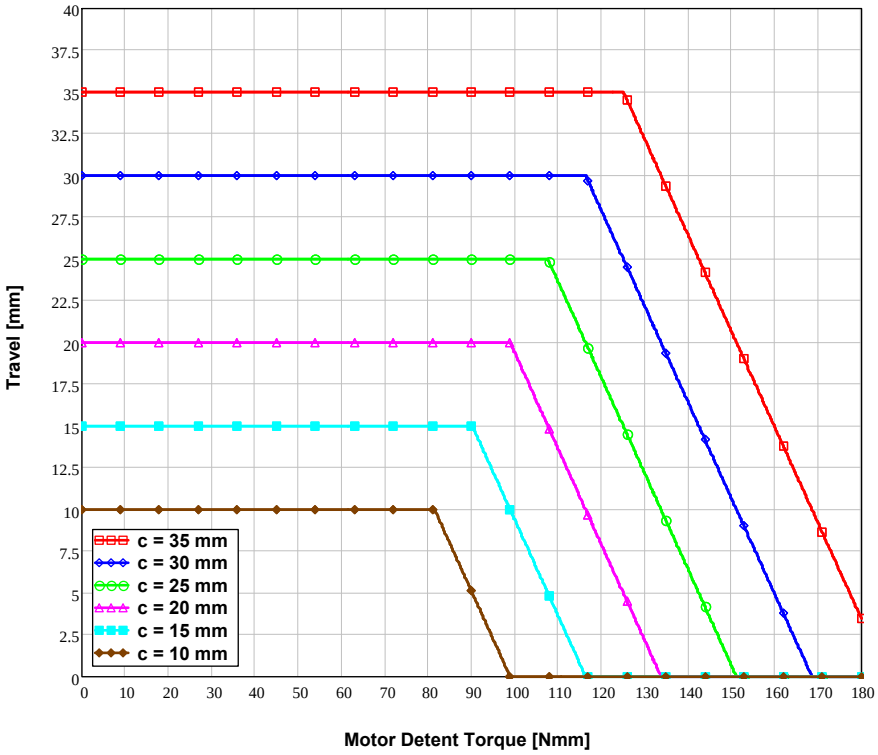

Figure 7-20 Dynamic reverse travel vs. detent torque with various initial positions (stiff springs, 0°)

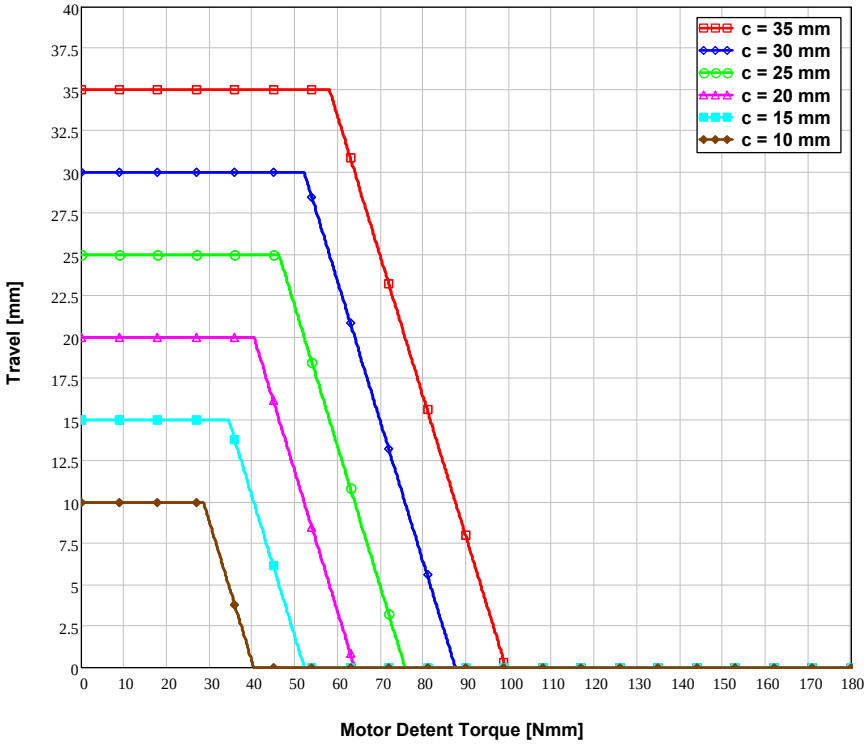

Figure 7-21 Dynamic reverse travel vs. detent torque with various initial positions (soft springs, 0°)

7.3.5 *Vertical TCTA - Soft springs(-90º) and stiff springs (+90º)*

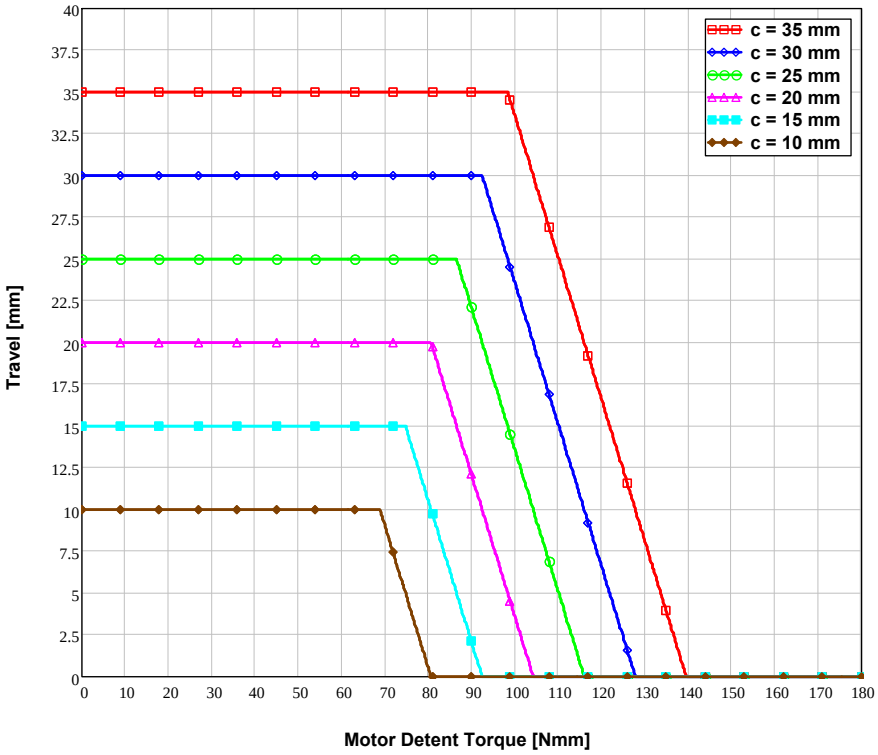

Figure 7-22 TCTA: dynamic reverse travel vs. motor detent torque (soft springs, -90º)

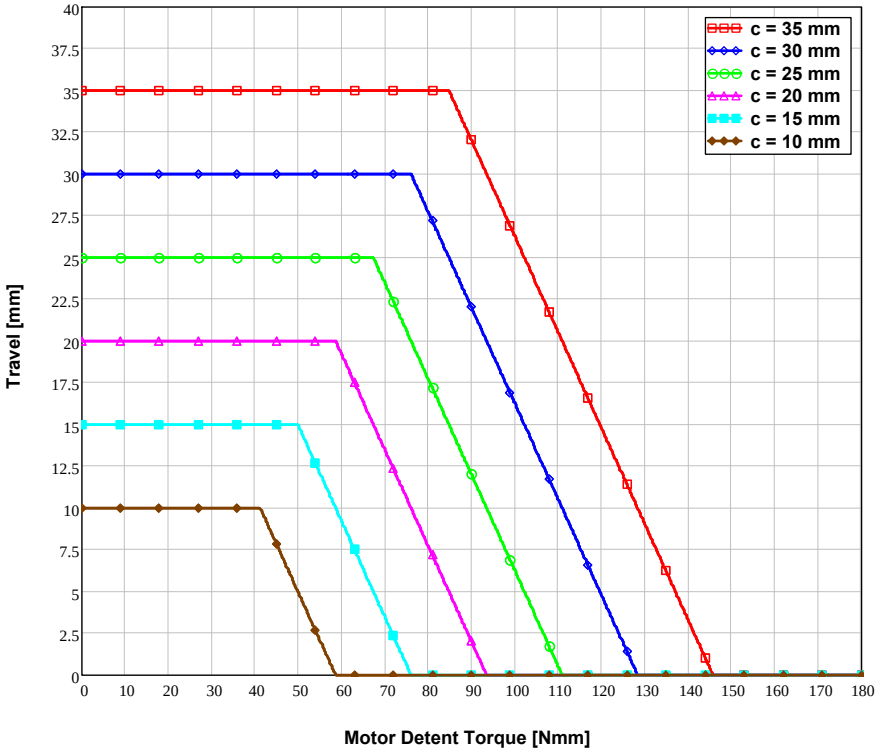

Figure 7-23 TCTA: dynamic reverse travel vs. motor detent torque (stiff springs, +90º)

7.4 Active absorbers (TCLA and TCLP)

Active absorbers are used in several locations of the LHC machine to absorb the remnants of the showers generated in the cleaning insertions (TCLA) and in the interaction regions of the two main experiments (IR1 and IR5 - TCLP).

From a mechanical point of view these devices share the same design, which is based on the TCSG but with an active jaw which is entirely made of OFE-Copper (with respect to the TCTA jaw - Figure 7-14 - the tungsten inserts are absent and replaced by solid copper). When it comes to the analysis of actuation system behaviour, the only difference with respect to TCTA and TCSG is then only the weight. The orientation of active absorbers is either horizontal or vertical.

7.4.1 Weight

The weight Q_j of TCLA/TCLP jaw assembly is **390 *N***. Weight of other mobile parts is given in Table 7-1.

7.4.2 Quasi-static forces

Plots of the quasi-static forces to drive in and back the jaw assembly are given in Figure 7-24 and Figure 7-25. Curves at 0º are the same as for TCSG since weight plays no role in quasi-static motion at this orientation.

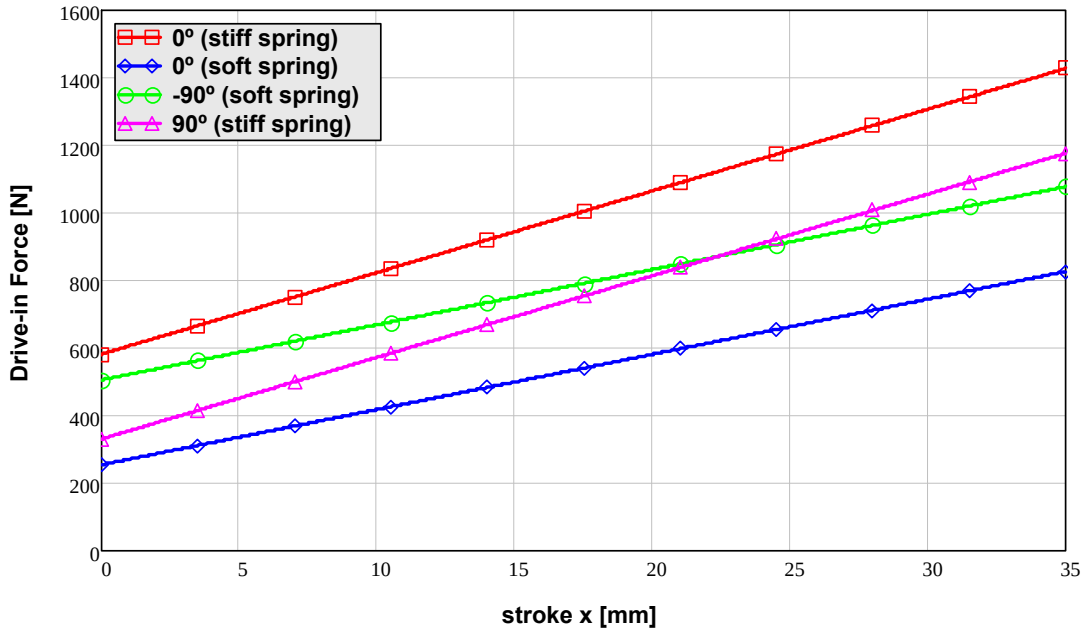

Figure 7-24 TCLA/TCLP: Quasi-static force required to drive in the jaw in various configurations

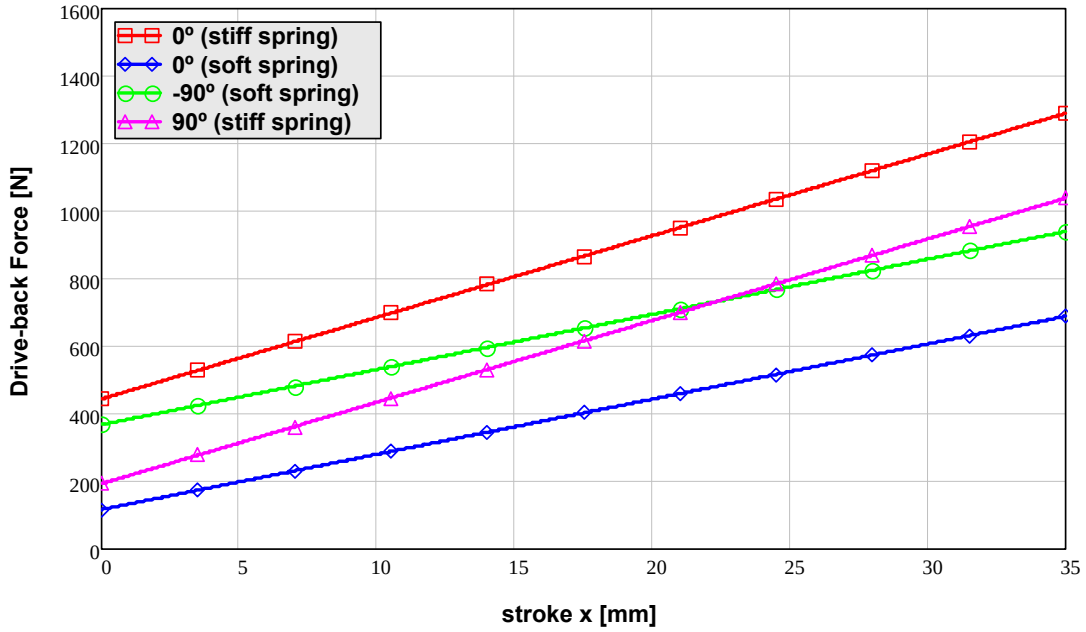

Figure 7-25 TCTA: Quasi-static back-driving force in various configurations

7.4.3 Quasi-static drive-in and drive-back torque

Figure 7-17 shows the torque required to drive in a TCTA jaw as a function of stroke in various configurations. In Figure 7-18 quasi-static back motion is described: positive torque indicates that the motor is braking to counteract the mechanical force pushing the jaw backwards.

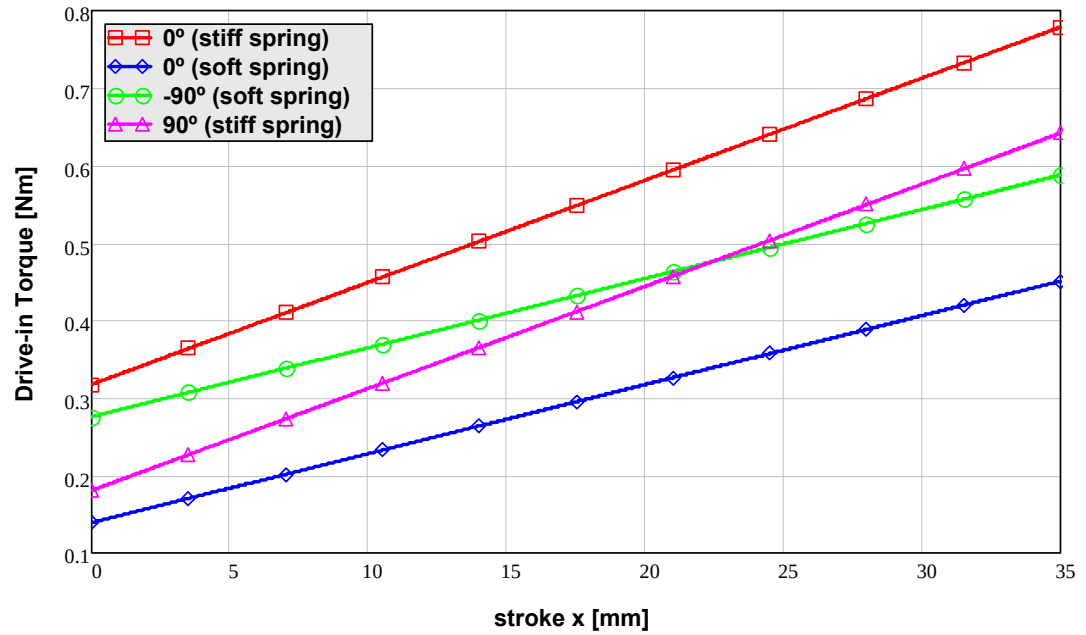

Figure 7-26 TCTA: Quasi-static motor torque $T_{qs}(x)$ required to drive-in the jaw as a function of stroke

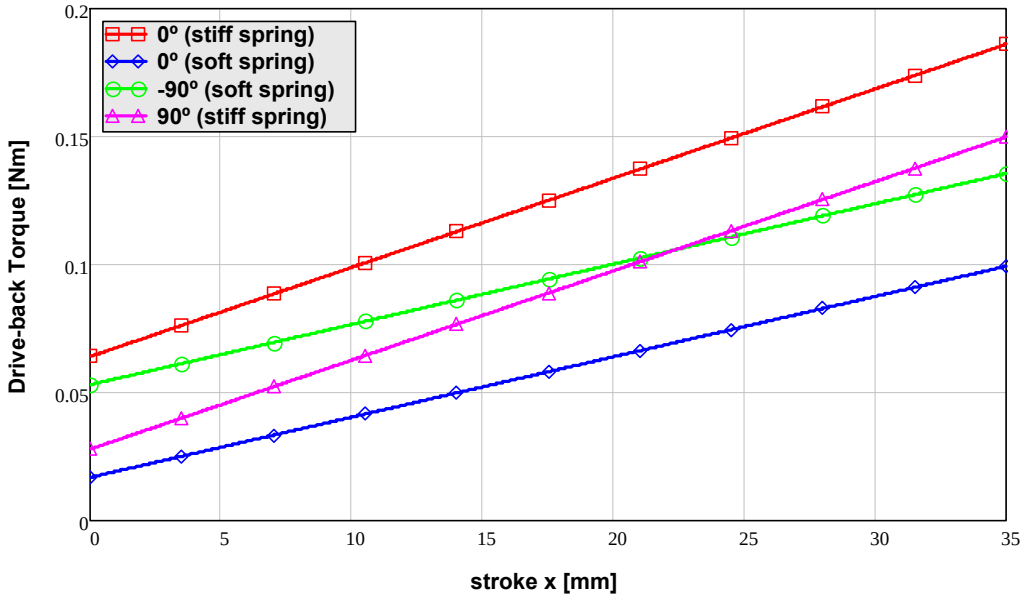

Figure 7-27 TCLA/TCLP: Quasi-static torque $T'_{qs}(x)$ to be supplied by the motor during back-driving

7.4.4 Dynamic analysis of auto-retraction

7.4.4.1 Horizontal TCLA/TCLP (0º) – Stiff and soft springs

As one can see, results are virtually identical to those of TCSG and TCTA for the same orientation: this is due to the predominant effect on the equivalent mass of the inertia of the rotating parts (in particular the motor rotor) with respect to the masses of jaw assemblies.

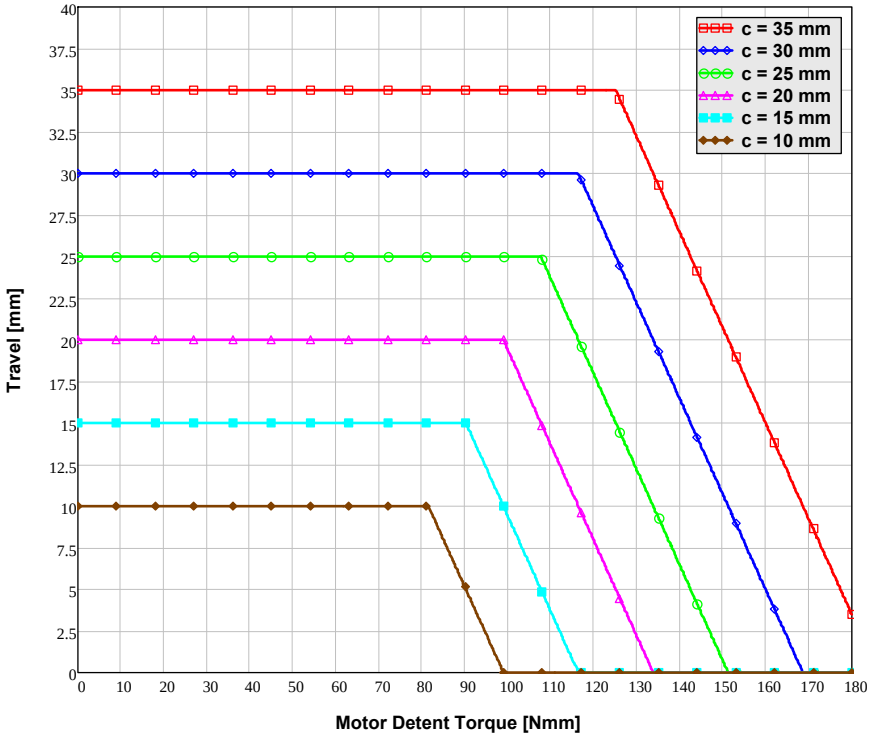

Figure 7-28 Dynamic reverse travel vs. detent torque with various initial positions (stiff springs, 0º)

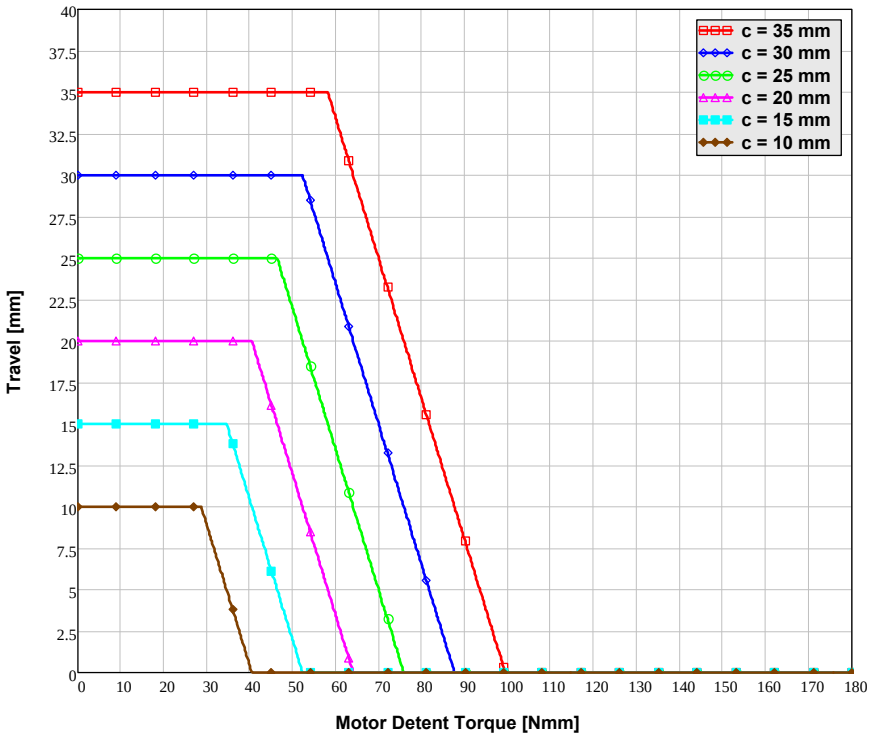

Figure 7-29 Dynamic reverse travel vs. detent torque with various initial positions (soft springs, 0º)

7.4.4.2 Vertical TCLP/TCLA - Soft springs(-90º) and stiff springs (+90º)

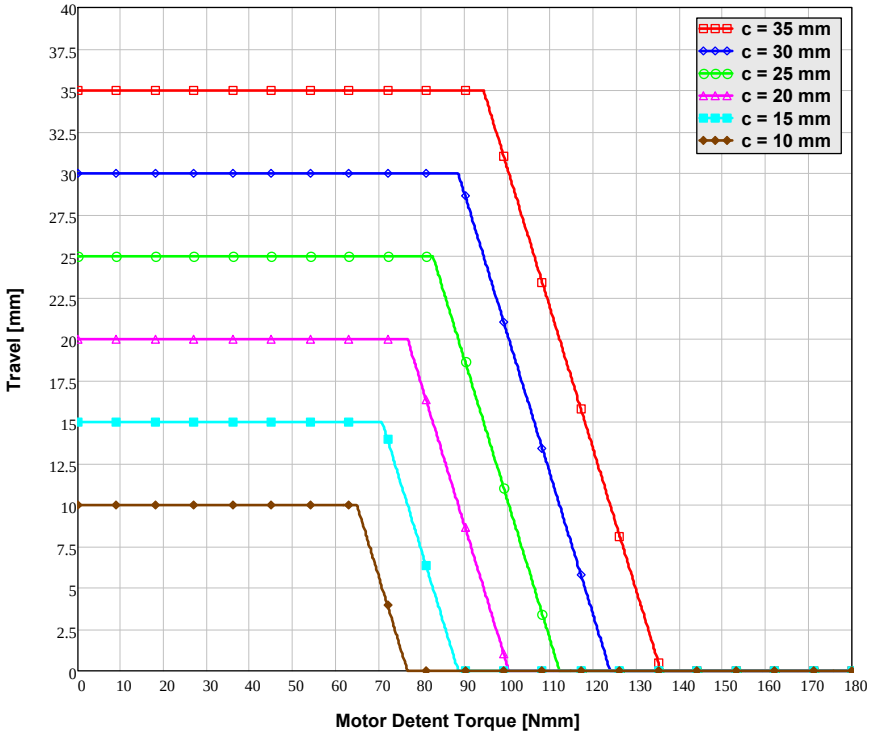

Figure 7-30 Dynamic reverse travel vs. motor detent torque (soft springs, -90º)

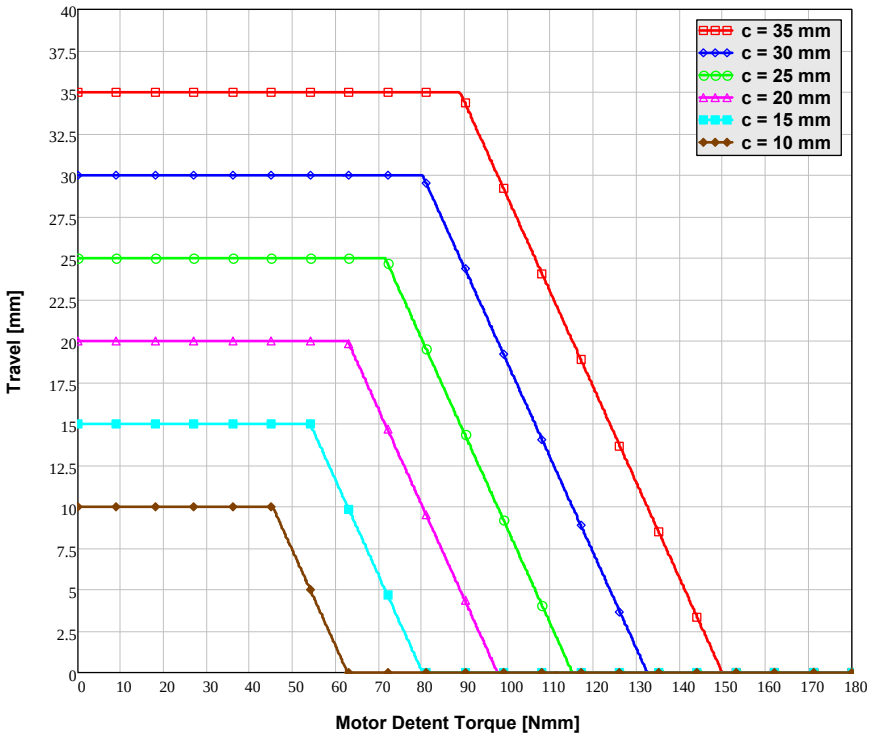

Figure 7-31 Dynamic reverse travel vs. motor detent torque (stiff springs, +90º)

7.5 Transfer Line Collimators (TCDI)

TCDI collimators were conceived to protect the equipment in the transfer lines, the LHC injection regions and the LHC machine against uncontrolled losses during beam injection into the LHC main ring. These collimators will be installed in the two transfer lines (TI 2 and TI 8), with vertical or horizontal orientation only (no skew collimators).

TCDI design is a simplified variant of the TCSG collimator: given the very low duty cycle of the injection lines, cooling is required neither for the jaw assembly nor for the vacuum tank. On a similar ground, the RF system is not implemented and the auto-retraction is not required.

These different requirements led to simpler design of the jaw assembly (which features a graphite jaw instead of Carbon/Carbon, while Glidcop is replaced by Stainless steel), while the high-efficiency roller screws of the mobile tables are replaced by a standard stainless steel screw (M14x2) and a brass nut. The screw is graphite coated and radiation-resistant grease is used.

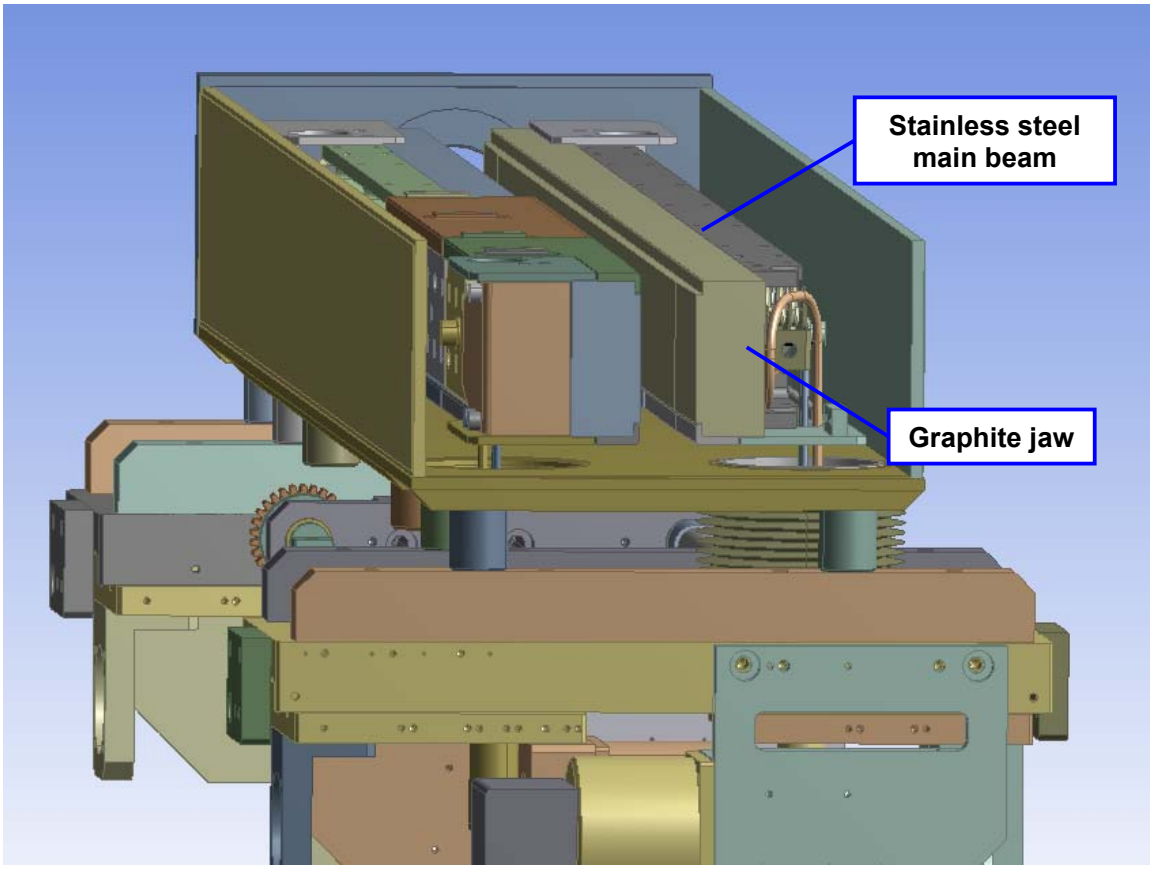

Figure 7-32: An open view of a TCDI collimator showing the jaw assembly

7.5.1 Weight

Weight of the jaw assembly and of the other mobile parts for a TCDI is given in Table 7-12

Assembly		***Weight [N]***
Q_j	*Jaw Assembly (Carbon/Carbon)*	*270*
Q_a	*Axle and mobile table components*	*110*

Table 7-9 Weights of jaw assembly, and axle and mobile parts

7.5.2 Return spring force

In TCDI case, return springs are only required to recover all mechanical plays, since auto-retraction is not required, hence softer springs can be chosen. However, to counteract the jaw assembly weight tending to move in the jaw at the full-out position a higher preload spring is used when $\beta=90^o$ to push up the jaw against the outer stop. On the other hand, when $\beta=-90^o$ springs are not required as gravity is sufficient to recover all plays in any jaw position without affecting calibration precision.

As for other collimators, maximum travel is 35 *mm*.

Spring type	Mean diameter D [mm]	Wire diameter d [mm]	Free length L_0 [mm]	Spring ratio K_r [N/mm]
VD-346 (low prealod)	50	5	130	7.955
VD-347 (high preload)	50	5	195	5.15
VD-315 (with roller screw)	50	4	150	3.258

Table 7-10 Return spring data for TCDI

7.5.3 Metric screw data

As said above a standard milled metric screw is used instead of a roller screw, since the system must be self-locking in reverse motion. Friction coefficient has been estimated on the basis of the nut material (brass) and of the screw material (stainless steel) and considering the effects of lubricants (i.e. graphite coating (Lubodry G) and radiation-hard grease as for a roller screw). Typical values for friction coefficients are given in ref. [16] – table A5. We assume the friction coefficient is in the high end of class C, i.e. **0.24**[9]. As it will be seen later, this parameter is extremely important, and if for any reason (e.g. bad alignment or out of tolerance dimensions) friction coefficient significantly increases, its effect on the actuation system might be very detrimental, possibly increasing required torque beyond available motor torque.

Nominal diameter d_0 [mm]	Pitch (mean) diameter d_2 [mm]	Lead p [mm]	Length L_s [mm]	Friction coefficient μ_s
14	12.701	2	135	0.24

Table 7-11 Parameters of TCDI power screw M14x2

7.5.4 Direct and indirect efficiency

For a metric screw, efficiency is given by the following formula [17]:

$$\eta = \frac{\tan(\alpha)}{\tan(\alpha + \varphi)}$$

[9] For conservaitive reasons, we have chosen here friction coefficient class C, ranging from 0.16 to 0.24 rather than class B (0.08 to 0.16), which given the lubricants used, may be considered more appropriate.

Where $\alpha = \frac{p}{2\pi d_2}$ is the lead angle of the thread and $\varphi = \arctan\left(\frac{\mu_s}{\cos(30^o)}\right)$ is the friction angle for a metric screw (thread angle is 60º).

Making use of the values provided in Table 7-14 we obtain $\boldsymbol{\eta = 0.151}$.

The indirect efficiency is given by:

$$\eta' = \frac{\tan(\alpha - \varphi)}{\tan(\alpha)}$$

It is immediate to realize that the screw is self locking, since indirect efficiency is less than zero ($\boldsymbol{\eta' = -4.467}$).

7.5.5 Quasi-static drive-in and drive-back torque

Figure 7-33 and Figure 7-34 show the torque required to drive in a TCDI jaw as a function of stroke for the different configurations. Plots are given for two different tank conditions in air and under vacuum: this affects the forces exerted by the bellows and may in some cases, as shown in Figure 7-34 (at 0º with VD-346), efface the preload in the full out position making calibration more complex. In this case we have a reversal of the force direction on the nut, switching from direct to indirect mode (then indirect efficiency must be used, explaining the change of sign in the slope). However, switch and stop calibration is usually done in the in-air condition, and in this case preload is always effective.

Although springs are not required at β=*-90º*, plots are given also for a soft spring in this configuration.

Maximum required torque (under vacuum) is ***1.55*** **Nm** for β=*-90º* (weight opening the jaw) if a VD-346 spring is used; otherwise maximum required torque is **1.19 Nm** for β=*90º* (weight closing the jaw) with a VD-347 spring.

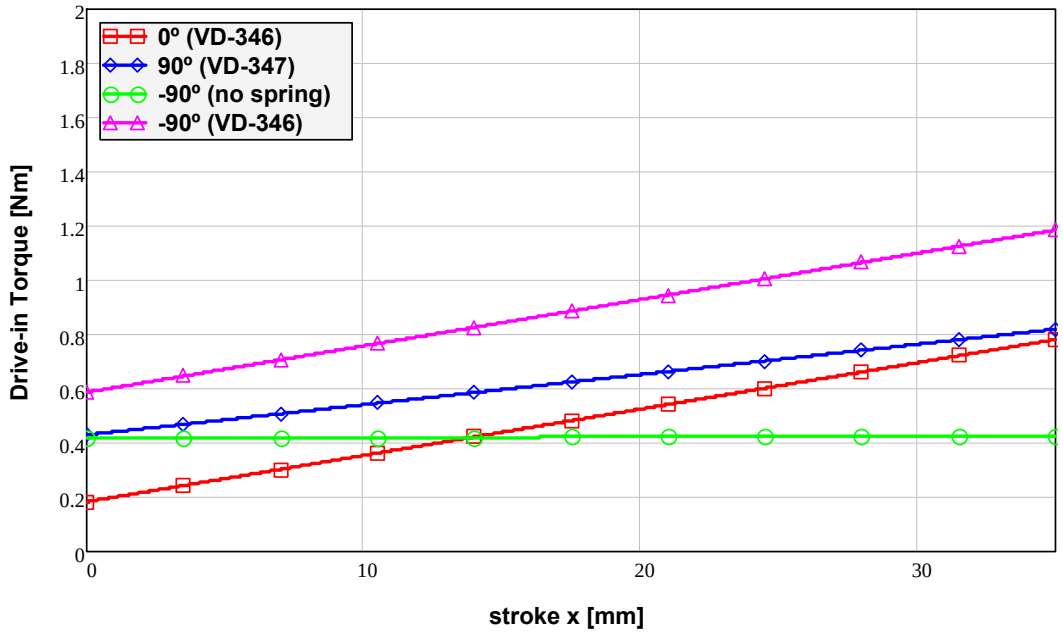

Figure 7-33: Drive-in torque for a TCDI in different configurations, tank in air (metric screw)

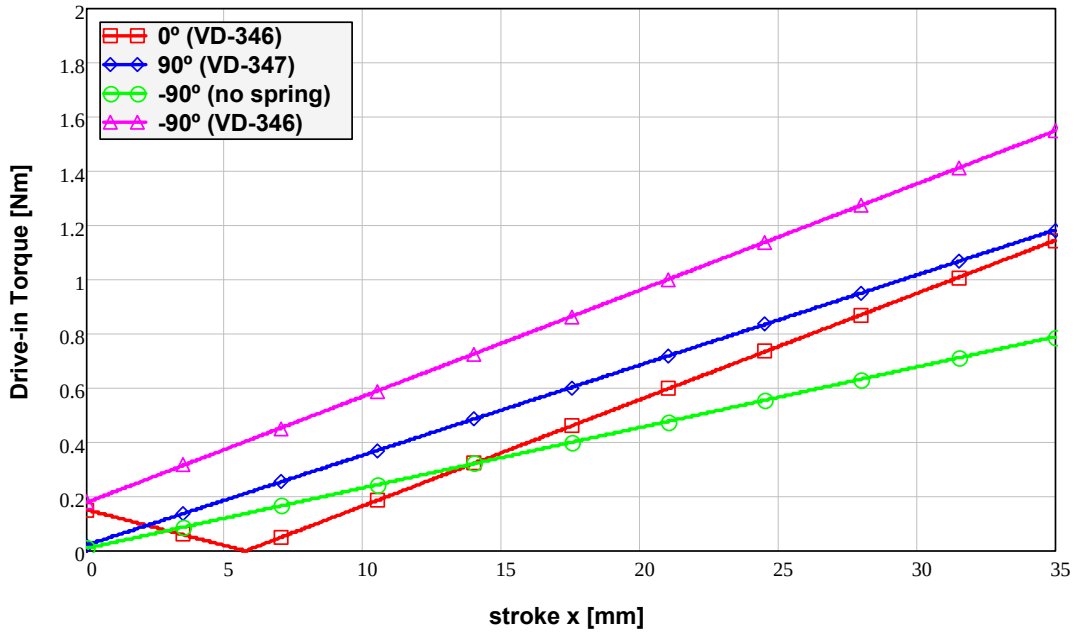

Figure 7-34: Drive-in torque for a TCDI in different configurations, tank under vacuum (metric screw)

Curves in Figure 7-35 and Figure 7-36 show the torque required to drive back the jaw assembly with tank in air and under vacuum. As expected this torque is always negative, i.e. the motor is always pulling back since the reverse efficiency of the system is negative (self-locking screw). Incidentally, we note that since indirect efficiency becomes negative, torque slope is opposed to that of drive-in torque except at the initial part of the travel at 0º under vacuum where force is inward directed so that the screw is working in direct mode.

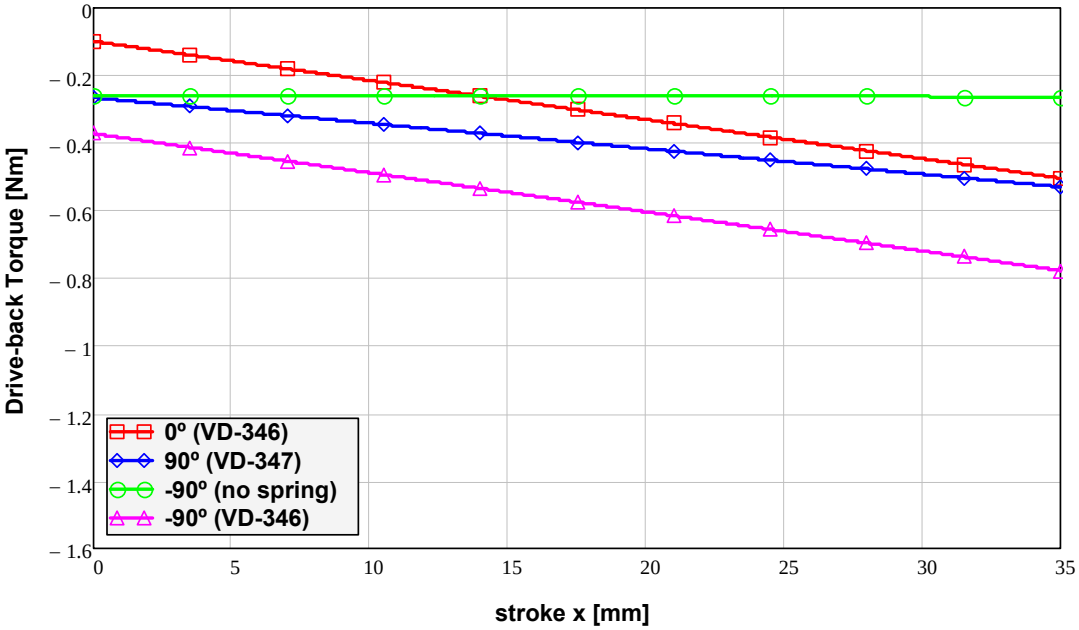

Figure 7-35: Back drive torque for a TCDI in different configurations, tank in air (metric screw)

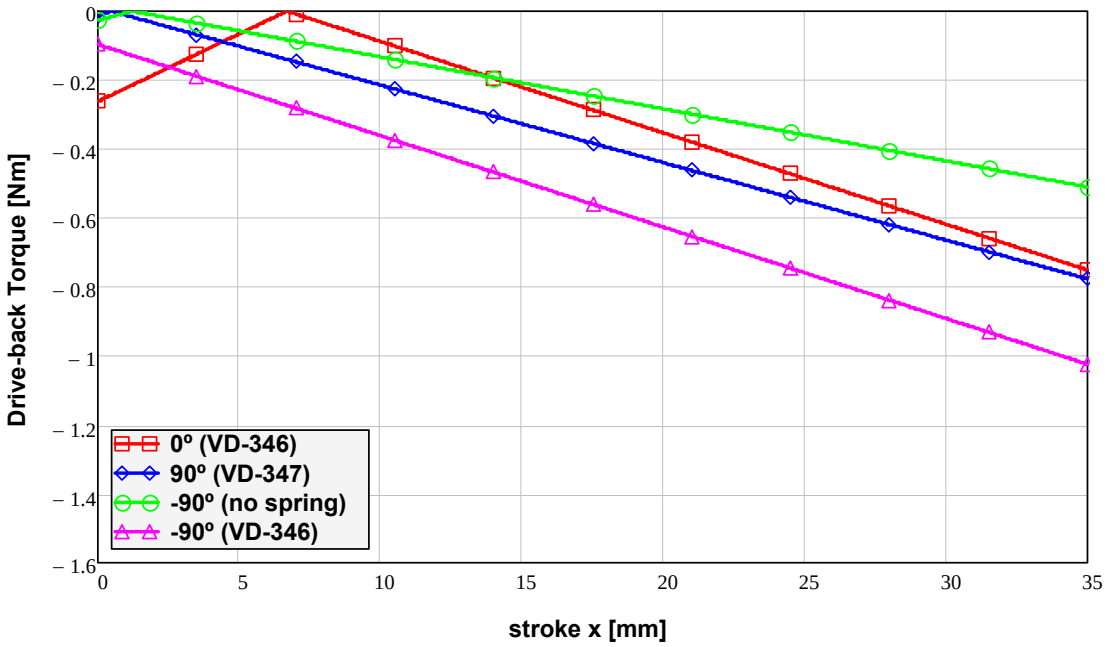

Figure 7-36: TCDI Drive-back torque in different configurations, tank under vacuum (metric screw)

If, to reduce the motor torque, one decides to use a roller screw instead of the metric screw, required torques are considerably reduced (Figure 7-37 and Figure 7-38) since efficiency is much higher and indirect efficiency is positive (making auto-retraction possible). As above, changes of slope are related to reversal of the force direction and switching from direct to indirect modes or vice-versa.

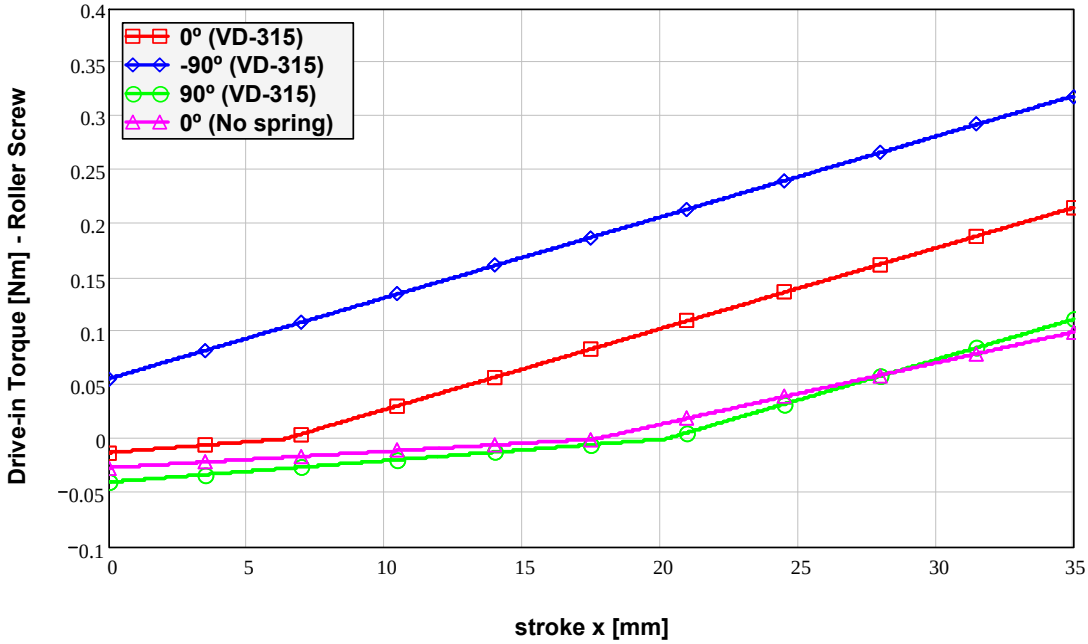

Figure 7-37: TCDI Drive-in torque using TCSG roller screws, under vacuum

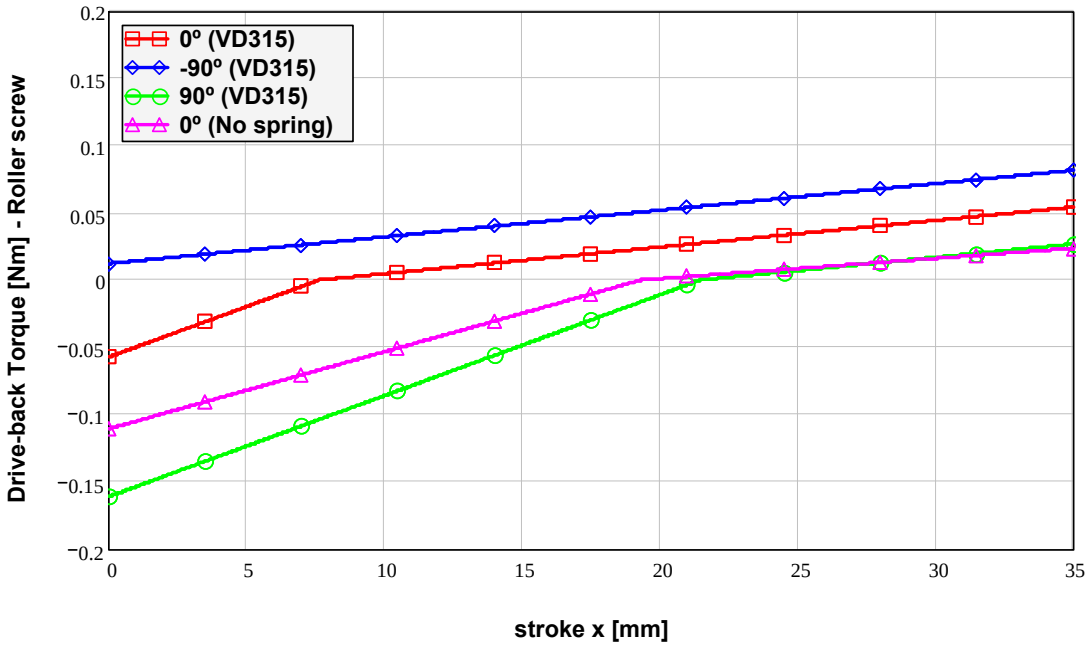

Figure 7-38 TCDI Drive-back torque using TCSG roller screw, under vacuum

7.5.6 Dynamic analysis of auto-retraction

In case a standard roller-screw is used, auto-retraction is possible in some cases. Figure 7-39 presents the most relevant case, i.e. -90º.

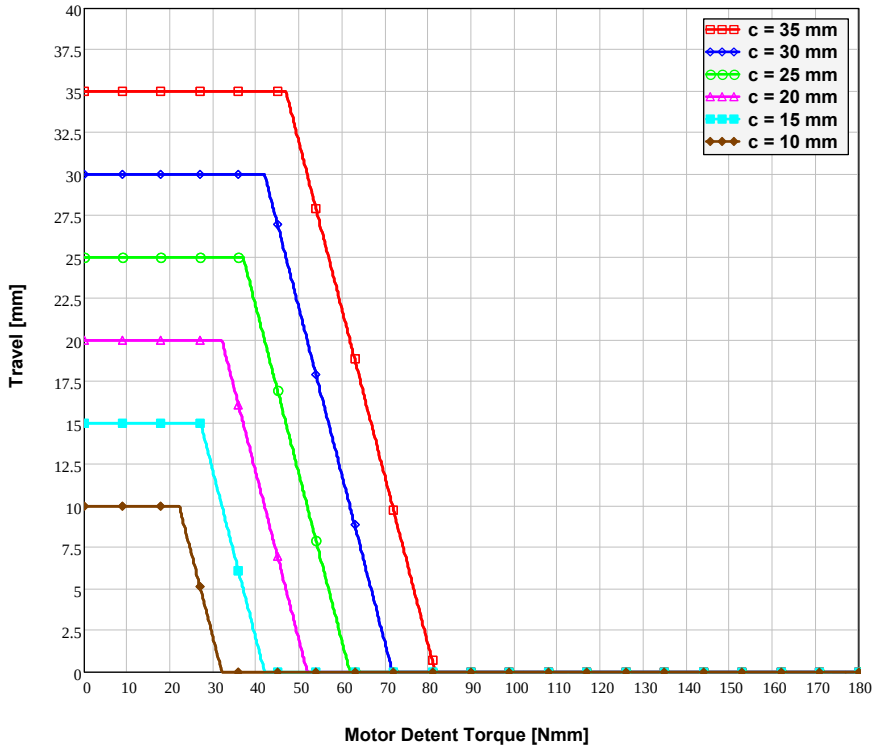

Figure 7-39: TCDI dynamic reverse travel as a function of Detent Torque with β = -90º

7.6 Injection protection collimators type A - TCLIA

Additional collimators, called TCLI, are required to protect the machine from mis-steered particles in IR2 and IR8, in case of errors by the MKI injection kickers. Where the space allowance is sufficient, the mechanical design exactly matches that of TCSG: these objects are known as TCLIB. However, in two required locations the beam pipes are too close to each other to allow a standard collimator to be accommodated in between; in these cases a special design is required, encompassing the two beams in a single collimator tank; these "two in one" injection protection collimators are called TCLIA.

A similar design is shared by the vertical tertiary collimators installed in locations nearby the TCLIA: these collimators are called TCTVB.

The TCLIA, shown in Figure 7-40, features quite a different design with respect to the TCSG. The tank is larger to fit in the two beams, while the jaw assembly has a reduced height and a more complex carbon/carbon jaw. In what concerns the actuation system, the main differences concern the shape and weight of the jaw assembly, the sliding table, which is larger, heavier and includes a different type of linear bearings[10] and a different roller bearing (four-contact ball bearing). The anti-misalignment system has been strengthened, with a stiffer stainless steel shaft (instead of aluminum alloy), a larger pinion and a larger rack; these modifications lead to a heavier equivalent mass of this system.

Another important difference is found in the RF contact system, which is more complex because of the much greater offset between jaw assembly and tank.

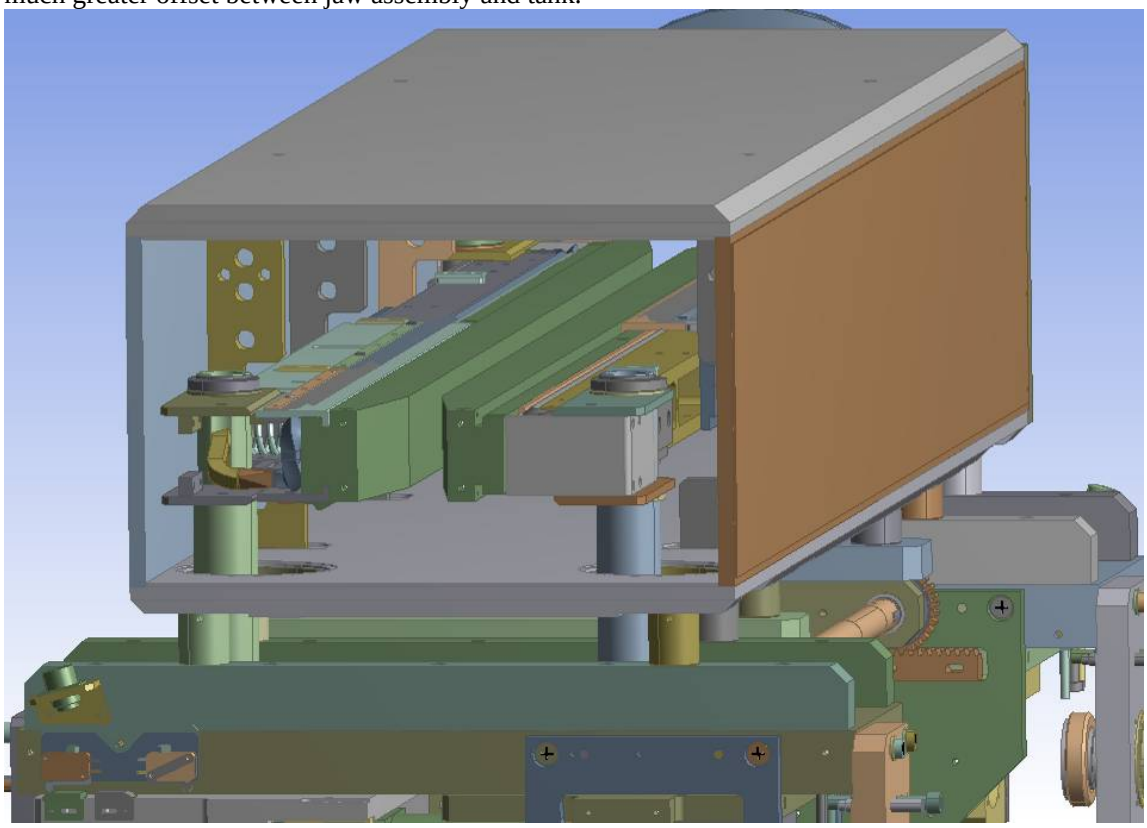

[10] The TCLIA /TCTVB linear bearings possess a particular feature, named Anti Cage-Creeping System (ACS), consisting in a miniaturized rack and pinion system, preventing the cage from sliding out of position in any condition

Figure 7-40: TCLIA general assembly (RF system not shown)

All other elements as springs, bellows, roller screws and RF contact are shared with the TCSG.

7.6.1 Weight

The weights of the jaw assembly and of the actuation system mobile parts are given in Table 7-12 .

Assembly		***Weight [N]***
Q_j	*TCLIA – Carbon/Carbon jaw*	*290*
Q_a	*Axle and mobile parts*	*155*

Table 7-12 Weights of TCLIA jaw assembly, axle and mobile parts

7.6.2 Linear bearing friction force

As said above, different general design of TCLIA and TCTVB with respect to baseline collimators led to the choice of stiffer and longer linear bearings for these collimators: the crossed-roller cage has been replaced by a needle cage (Figure 7-41). The linear bearing is equipped with an all-metal *anti-creep system* (ACS) made up by two small pinions mounted in a dedicated groove at the centre of the brass needle cage and engaged between two racks fit into the V-shaped and M-shaped rails. This solution prevents the cage from creeping with respect to its nominal position, without interfering with the regular movement of the bearing, since the pinions move at the same speed of the cage (i.e. half the speed of the mobile rail). All ACS components are made of brass. Details of each ACS component are shown in Figure 7-42: parts of the depicted components are coated with a graphite-based dry lubricant in view of specific tests to assess its compatibility with a radioactive environment. These tests ruled out the possibility to use such lubricant since radiation fosters the corrosion of brass in presence of graphite [9]. Other linear bearing components are made of corrosion resistant steel.

Table 7-13 shows relevant data for the Anti-Creeping System according to [11].

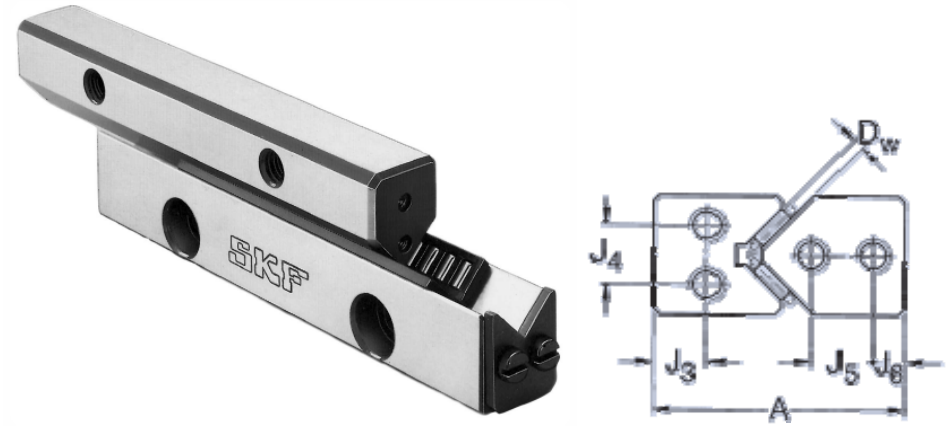

Figure 7-41 Typical mounting arrangement of needle cage linear bearings (no ACS featured)

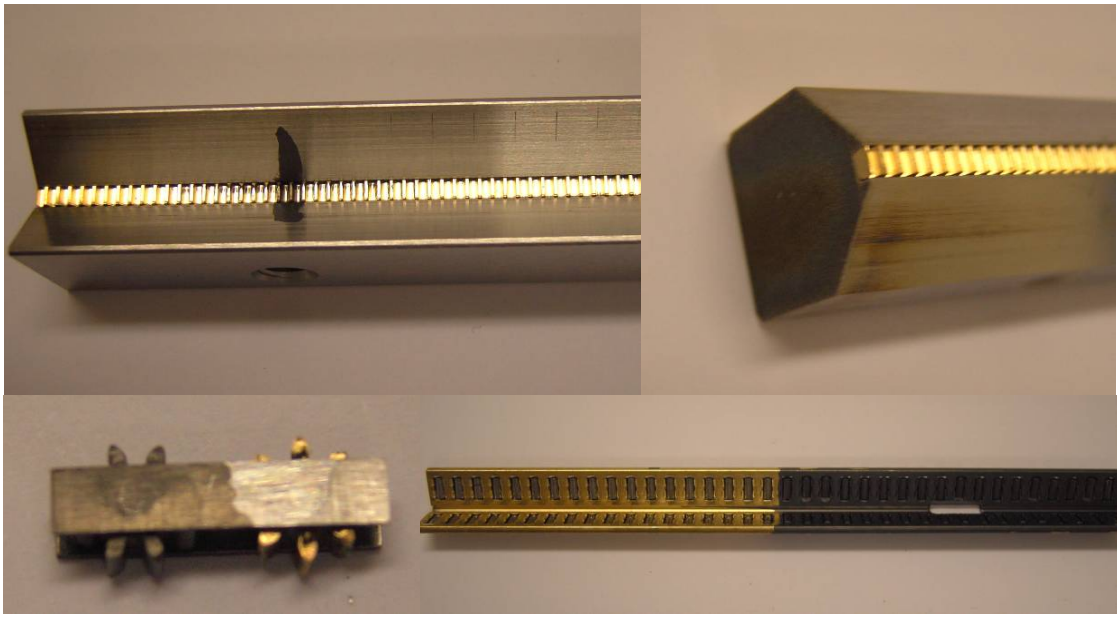

Figure 7-42 Pictures of the linear bearing ACS system, showing the racks mounted into the rails, the pinion assembly and the needle roller cage with the groove where pinions are inserted

Max friction coefficient η_t	Length of the cage [mm]	Permissible load per Roller C [N]	Allowable preload per roller p_r [%]	Roller pitch t [mm]	Distance between set-screws L_1 [mm]
0.003	225	530	10	4	50

Table 7-13 Linear bearing data – SKF assembly type LWR6 (rail1 M 6250/03/E1/HV/ACSM, rail2 V 6200/03/E1/HV/EG/ACSM, cage 10x225/MS/G2/HV/ACSM/MS)

The values of the quantities presented in Table 7-14, namely n_r, F_{vs}, F_{rt}, M_{vs} are calculated according to equations (9) to (14), section 3.1.4 taking into account data from Table 7-13.

Number of active roller pairs per screw n_r	Maximum preload force per screw F_{vs} [N]	Maximum preload force per rail F_{rt} [N]	M6 tightening coefficient a_{vs} [cm]	Required tightening torque M_{vs} [Nm]	Friction force per table F_{ft} [N]
12	1272	6360	0.0699	0.89	38.8

Table 7-14 Calculated quantities for the linear bearing - type SKF LWR6

7.6.3 Quasi-static forces

Only two TCLIA are foreseen in the LHC (one in IR2 and one in IR8), both with vertical orientation. Figure 7-43 and Figure 7-44 show the quasi-static forces required to drive-in and drive-back the jaw.

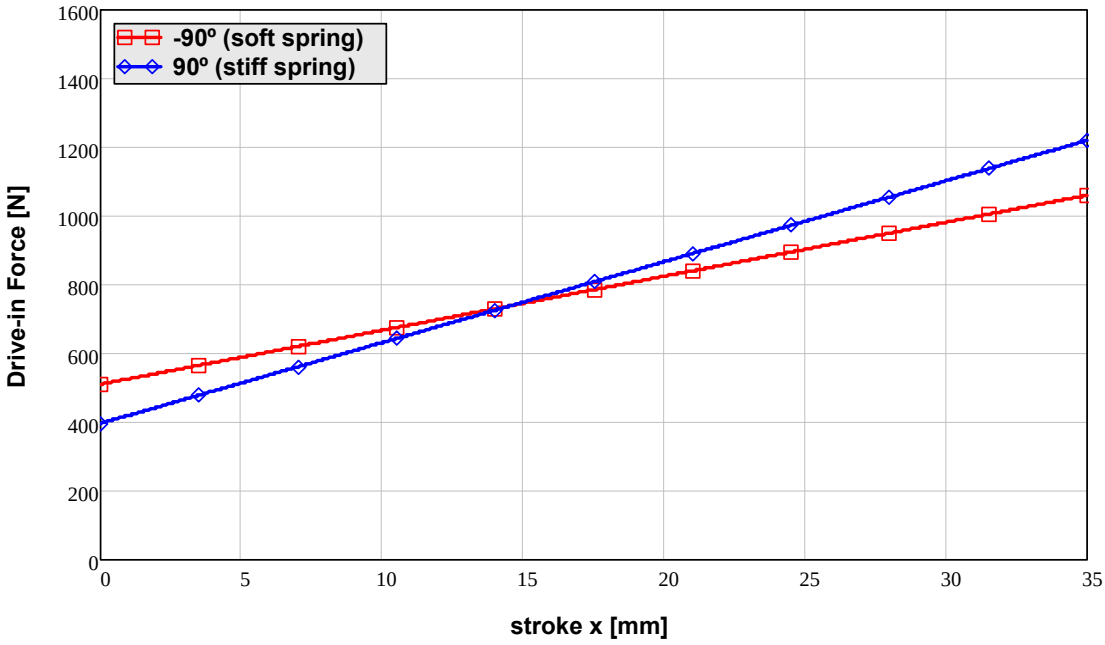

Figure 7-43 TCLIA: Total quasi-static force required to drive in the jaw

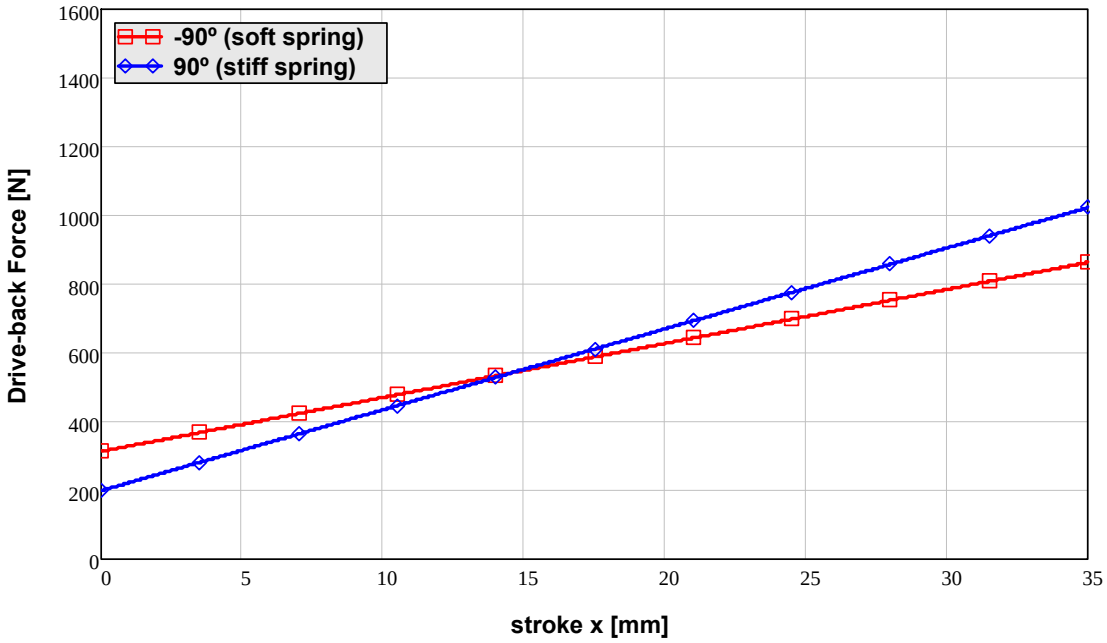

Figure 7-44: TCLIA: Total quasi-static force required to drive back the jaw

7.6.4 Bearing friction moment

On the fixed end the TCLIA roller screw is borne by a 4-contact ball bearing 20x52x15 SKF QJ304 [13].

Relevant data to compute the friction moment induced by this bearing (according to equations (45) and (46)) are given in Table 7-15 [18].

Inner diameter d [mm]	Outer diameter D [mm]	Width B [mm]	Basic static load ratings C_0 [kN]	Friction coefficient μ
20	52	15	18.3	0.0016

Table 7-15 Four-point contact ball bearing 20x52x15 SKF QJ304

7.6.5 Quasi-static drive-in and drive-back torque

Drive-in and drive-back torques in quasi-static conditions are plotted in Figure 7-45.

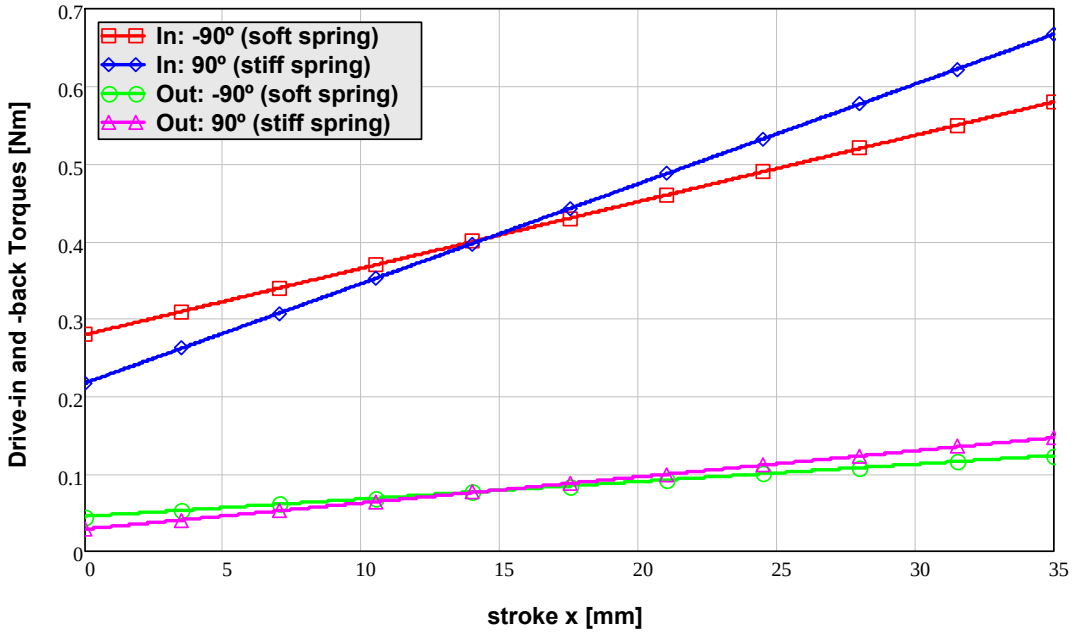

Figure 7-45 TCLIA: Quasi-static motor torque $T_{qs}(x)$ and $T'_{qs}(x)$ required to drive-in and back the jaw.

7.6.6 Dynamic analysis of auto-retraction

The expected behavior of the TCLIA collimator in case of auto-retraction is presented for the two cases (-90º and 90º) with stiff and soft springs in Figure 7-46 and Figure 7-47 respectively

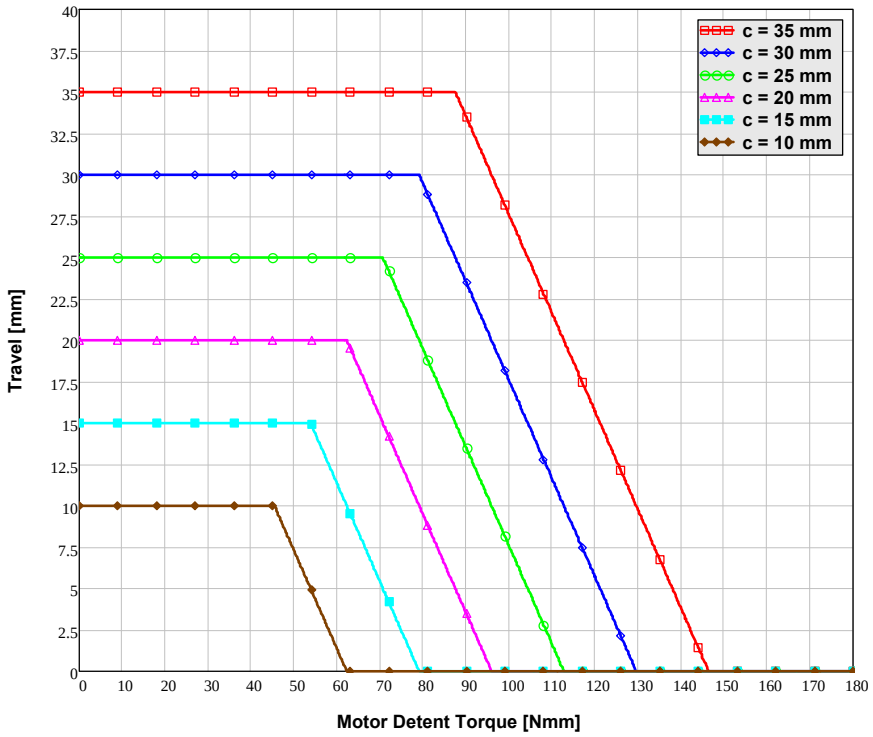

Figure 7-46 TCLIA: Dynamic reverse travel vs. Detent Torque with various initial positions (stiff springs, +90º)

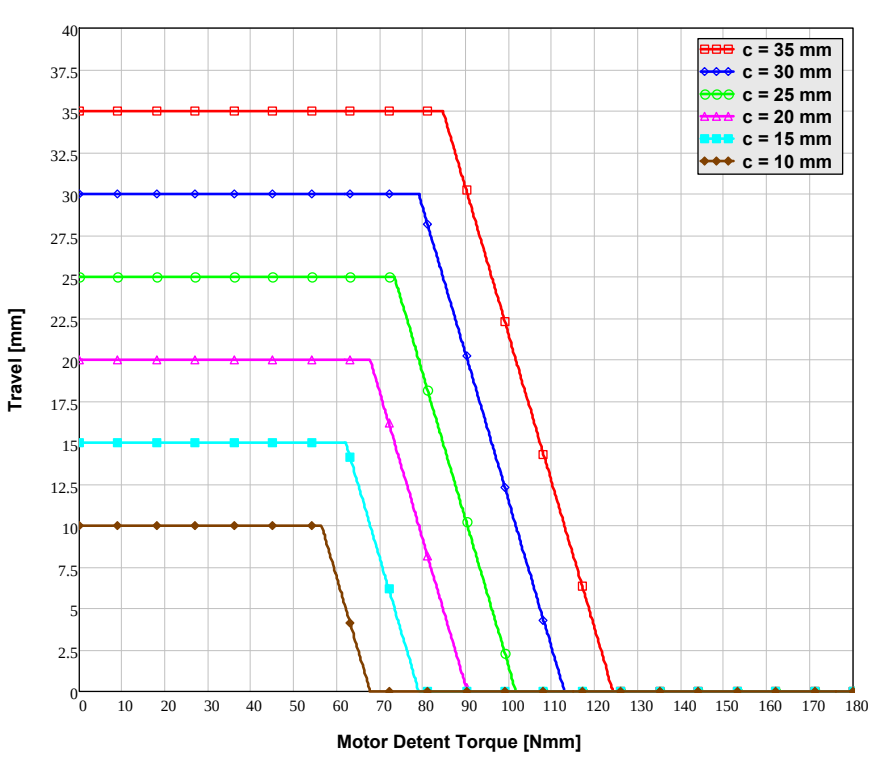

Figure 7-47 TCLIA: Dynamic reverse travel vs. Detent Torque with various initial positions (soft springs, -90º)

7.7 Tertiary collimators type B - vertical (TCTVB)

As said above TCTVB are special tertiary collimators installed in IR2 and IR8 in locations where the two beams are too close to use a standard vacuum vessel. They share therefore the same general design of the TCLIA, with a different jaw (an all-metal tungsten/copper jaw is used instead of carbon/carbon). All TCTVB units are mounted in vertical position.

7.7.1 Weight

The weights of the jaw assembly and of the actuation system mobile parts (same as TCLIA) are given in Table 7-16.

Assembly		***Weight [N]***
Q_j	*TCTVB – Tungsten/Copper jaw*	*500*
Q_a	*Axle and mobile parts*	*155*

Table 7-16 Weights of TCTVB jaw assembly, axle and mobile parts

7.7.2 Quasi-static forces

Figure 7-48 shows the quasi-static forces required to drive-in and drive-back the jaw.

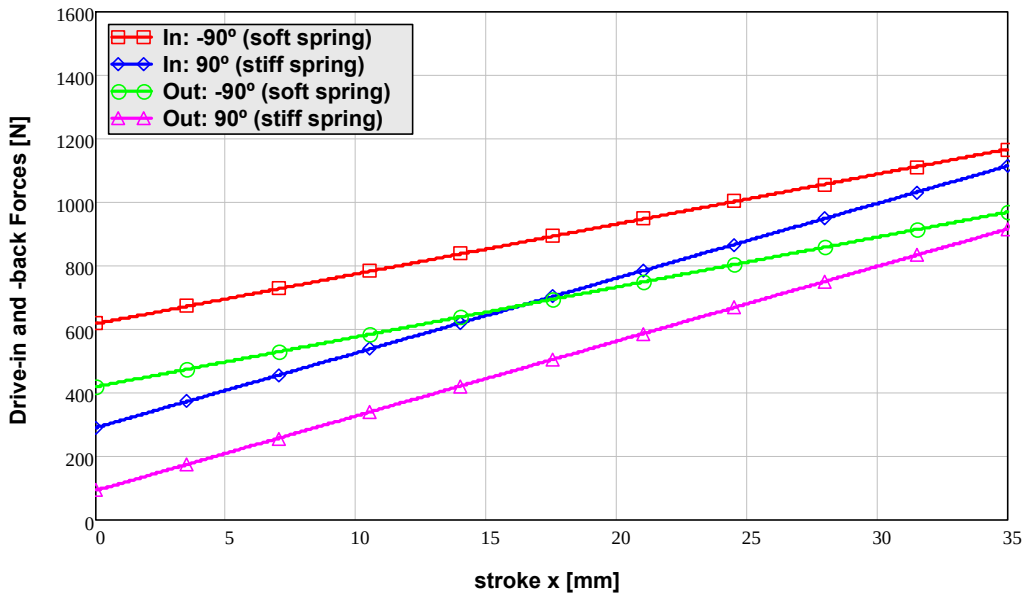

Figure 7-48 TCTVB: Total quasi-static forces required to drive in and back the jaw

7.7.3 Quasi-static drive-in and drive-back torque

Drive-in and drive-back torques in quasi-static conditions are plotted in Figure 7-45.

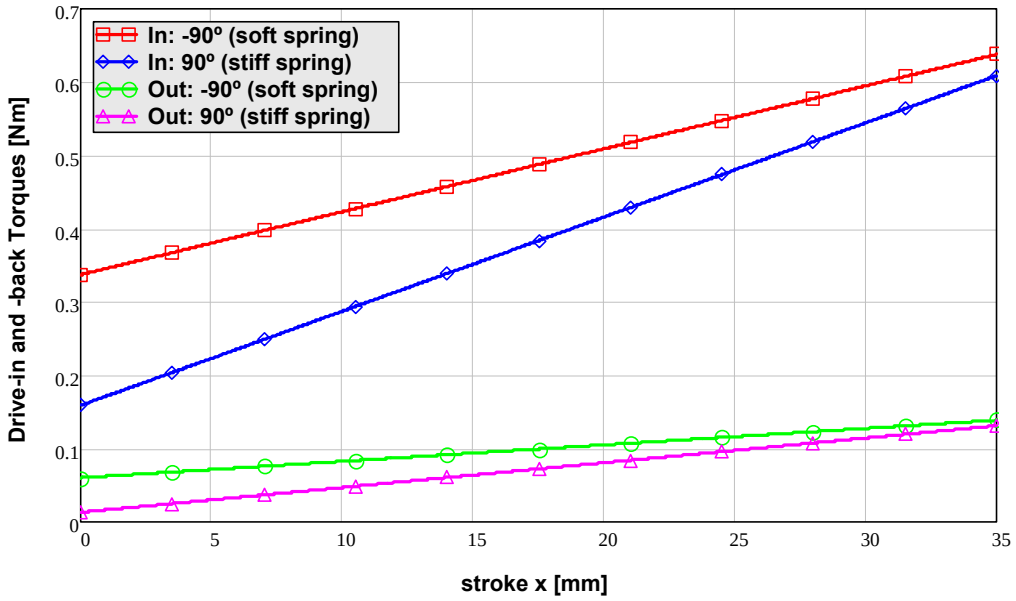

Figure 7-49 TCTVB: Quasi-static motor torque $T_{qs}(x)$ and $T'_{qs}(x)$ required to drive-in and back the jaw.

7.7.4 Dynamic analysis of auto-retraction

The expected behavior of the TCTVB collimator in case of auto-retraction is presented for the two cases (-90º and 90º) with stiff and soft springs in Figure 7-50 and Figure 7-51 respectively.

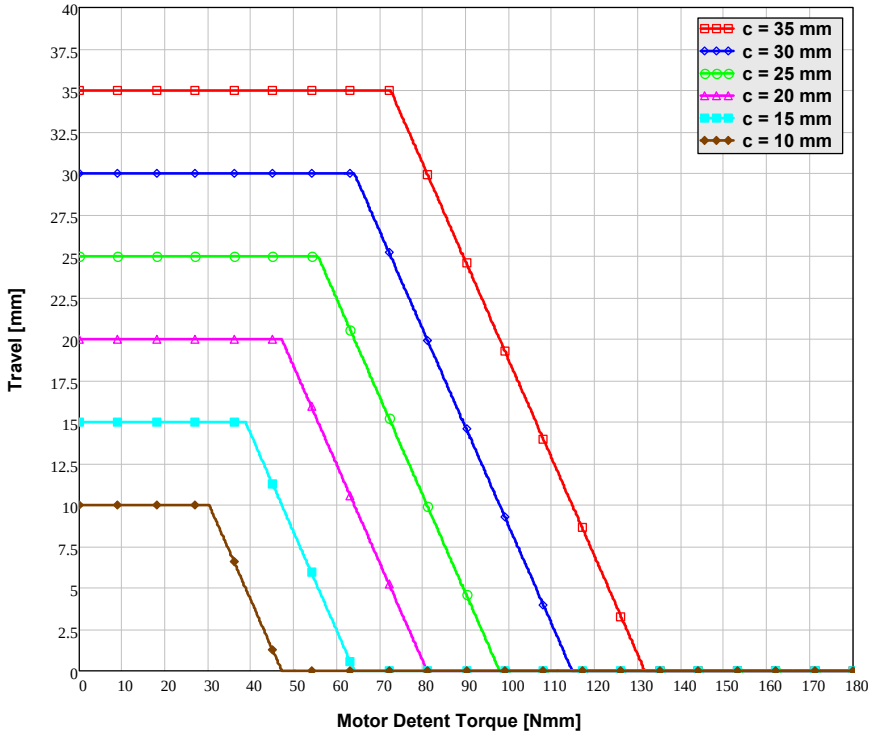

Figure 7-50 TCTVB: Dynamic reverse travel vs. Detent Torque with various initial positions (stiff springs, +90º).

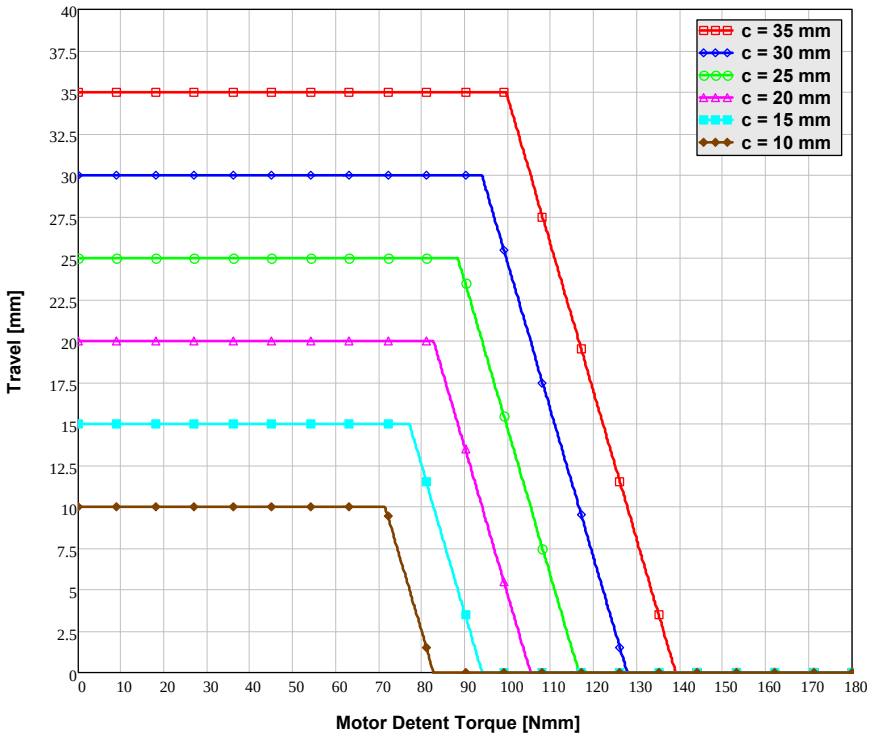

Figure 7-51 TCTVB: Dynamic reverse travel vs. Detent Torque with various initial positions (soft springs, -90º)